



HAL
open science

Laser-Induced Breakdown Spectroscopy (LIBS) characterization of granular soils: Implications for ChemCam analyses at Gale crater, Mars

Gael David, P-y Meslin, E Dehouck, O Gasnault, A Cousin, O Forni, G
Berger, J Lasue, P Pinet, R C Wiens, et al.

► **To cite this version:**

Gael David, P-y Meslin, E Dehouck, O Gasnault, A Cousin, et al.. Laser-Induced Breakdown Spectroscopy (LIBS) characterization of granular soils: Implications for ChemCam analyses at Gale crater, Mars. *Icarus*, 2021, *Icarus*, 365, pp.114481. 10.1016/j.icarus.2021.114481 . hal-03441476

HAL Id: hal-03441476

<https://hal.science/hal-03441476>

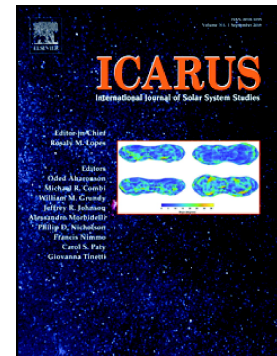
Submitted on 22 Nov 2021

HAL is a multi-disciplinary open access archive for the deposit and dissemination of scientific research documents, whether they are published or not. The documents may come from teaching and research institutions in France or abroad, or from public or private research centers.

L'archive ouverte pluridisciplinaire **HAL**, est destinée au dépôt et à la diffusion de documents scientifiques de niveau recherche, publiés ou non, émanant des établissements d'enseignement et de recherche français ou étrangers, des laboratoires publics ou privés.

Laser-Induced Breakdown Spectroscopy (LIBS) characterization of granular soils: Implications for ChemCam analyses at Gale crater, Mars

G. David, P.-Y. Meslin, E. Dehouck, O. Gasnault, A. Cousin, O. Forni, G. Berger, J. Lasue, P. Pinet, R.C. Wiens, S. Maurice, J.F. Fronton, W. Rapin



PII: S0019-1035(21)00161-5

DOI: <https://doi.org/10.1016/j.icarus.2021.114481>

Reference: YICAR 114481

To appear in: *Icarus*

Received date: 3 March 2020

Revised date: 19 February 2021

Accepted date: 15 April 2021

Please cite this article as: G. David, P.-Y. Meslin, E. Dehouck, et al., Laser-Induced Breakdown Spectroscopy (LIBS) characterization of granular soils: Implications for ChemCam analyses at Gale crater, Mars, *Icarus* (2018), <https://doi.org/10.1016/j.icarus.2021.114481>

This is a PDF file of an article that has undergone enhancements after acceptance, such as the addition of a cover page and metadata, and formatting for readability, but it is not yet the definitive version of record. This version will undergo additional copyediting, typesetting and review before it is published in its final form, but we are providing this version to give early visibility of the article. Please note that, during the production process, errors may be discovered which could affect the content, and all legal disclaimers that apply to the journal pertain.

Laser-Induced Breakdown Spectroscopy (LIBS) characterization of granular soils: implications for ChemCam analyses at Gale crater, Mars.

G. David^{1*}, Gael.david@irap.omp.eu, P-Y. Meslin¹, E. Dehouck^{1,2}, O. Gasnault¹, A. Cousin¹, O. Forni¹, G. Berger¹, J. Lasue¹, P. Pinet¹, R. C. Wiens³, S. Maurice¹, J.F. Fronton⁴, W. Rapin⁵

¹Institut de Recherche en Astrophysique et Planétologie, Université de Toulouse, CNRS, CNES, Toulouse, France,

²Univ Lyon, Univ Lyon 1, ENSL, CNRS, LGL-TPE, F-69622, Villeurbanne, France

³Los Alamos National Laboratory, Los Alamos, New Mexico, USA

⁴Centre National d'Etudes Spatiales, Toulouse, France

⁵California Institute of Technology, Division of Geological and Planetary Sciences, Pasadena, CA, USA

*Corresponding author.

Abstract

The Curiosity rover has been characterizing mineralogical and chemical compositions of Gale crater soils on Mars since 2012. Given its sub-millimeter scale of analysis, the ChemCam instrument is well suited to study the composition of soil constituents. However, the interpretation of LIBS data on soils in the martian environment is complicated by the large diversity of particle sizes (from dust to sand), combined with the unknown physical arrangement of their mineral constituents (i.e., the type of grain mixtures). For example, martian soils contain a significant amount of X-ray amorphous materials whose physical form remains unclear. In this study, we reproduced martian soil analyses in the laboratory to understand how the LIBS technique can provide specific insights into the physical and chemical properties of granular soils. For this purpose, different types of samples were studied with various ranges of grain sizes, mimicking two possible mixtures that may occur in martian soils: mechanical mixtures of two populations of grains made of distinct chemical compositions; and material forming a compositionally distinct coating at the surface of grains. Our results, also supported by *in situ* ChemCam data, demonstrate that both the sizes and the type of mixture of soil particles have a strong influence on the LIBS measurement. For mechanical mixtures of two populations of grains larger than 125-250 μm , the scatter of the data provides information about the chemical composition of the end-members. On the other hand, the chemistry recorded by LIBS for grains with surface coatings is fully dominated by the outer material for grains smaller than 500 μm in diameter. This is due to the small penetration depth of the laser (~ 0.3 -1.5 μm per shot), combined with the ejection of small grains at each shot, which leads to a constant replenishment of fresh material. This experimental work will thus improve our understanding of martian soils analyzed by ChemCam, and more broadly, will benefit LIBS studies of granular materials.

Keywords

Martian soil, Laser-Induced-Breakdown spectroscopy, Granular media, Planetary pedology, Independent Component analysis

1. Introduction

1.1 Martian soil observations

The surface of Mars is globally dominated by basaltic rocks, as successively shown by telescopic, orbital and *in situ* observations (e.g., Pinet and Chevrel, 1990; Christensen et al., 2000; Bandfield, 2002; McSween et al., 2004; Gasnault et al., 2010). Over time, these primary materials have undergone physical and chemical weathering, and have been partially turned into loose sediments, referred to as “soils” on Mars. Soils are considered as representative of the average martian crust after correcting for meteoric contributions (Taylor and McLennan, 2009, see Table 1). Indeed, they are thought to have sampled broad areas and large volumes of the exposed martian crust that have undergone variable degrees of chemical weathering and aqueous alteration as they are aggregates of local, regional, and global sources. In the context of *in situ* missions, the chemical composition of soils is accessible to rover analyses and they are particularly useful to characterize the alteration of the crust. Indeed, soil compositions may differ from pristine basalts due to the addition of volcanoclastic materials (that may be from different igneous provenances; Le Deit et al., 2016; Bedford et al., 2019) and secondary phases (McGlynn et al., 2011, and references therein). Due to their small size and large reactive surfaces compared to rocks, soils are also particularly effective in recording aqueous alteration processes during pedogenesis (McSween et al., 2010). The term “soil” in the context of martian studies is free of any biologic connotation and simply refers to all unconsolidated loose material, which can be distinguished from hardened rocks (Meslin et al., 2013). They consist of surficial deposits of fine-grained components mixed with rock fragments (Certini et al., 2020). It is important to make a distinction between soils and dust, although the boundary between both is sometimes difficult to define. It is mainly a particle size criterion. Dust often refers to particles smaller than a few micrometers in size that can be easily mobilized by the wind (Lasue et al., 2018), whereas the more general concept of soil encompasses micrometer- to millimeter-sized grains.

As seen from the ground, dust and soils seem to share a relatively similar chemical composition (Berger et al., 2016). Relative to soils, the dust has higher sulfur and chlorine abundances, but the S/Cl ratios are comparable (~3.7), suggesting that dust and soil formation may be genetically linked (Berger et al., 2016). Dust formation probably implies wind abrasion of soft rock units and the aeolian breakdown of saltating sand-sized particles (e.g., Ojha et al., 2018). However, dust is not the most chemically altered component of the martian soils, and although dust may be a contributor to the amorphous component found in soils, some differences in composition indicate that the two materials are not equivalent (Lasue et al., 2018).

The chemical composition of martian soils seems to be relatively homogeneous among the different landing sites. Indeed, the two Viking landers first highlighted the similar bulk soil compositions of the Chryse Planitia and Utopia Planitia soils (Clark et al. 1977). Apart from slightly lower alkaline elements and higher silica, Sojourner (Mars Pathfinder) in Ares Vallis also measured a similar composition (Brückner et al., 2003; Foley et al., 2003). The Fe and Mg enrichments in soils compared to the neighboring bedrocks suggested that soil compositions are not entirely controlled by alteration of local rocks in this region. The

Gusev crater and Meridiani Planum landing sites, respectively studied by the Spirit and Opportunity rovers, also revealed very concordant basaltic compositions (Gellert et al., 2004; Yen et al., 2005), consistent with orbital data from the Gamma-ray spectrometer onboard Mars Odyssey (Newsom et al., 2007). Consequently, soils seem to be quite uniform over these different landing sites with an influence of local rock chemistry (e.g., Yen et al., 2005). The relative chemical homogeneity of soils could be due to large-scale eolian mixing, or/and it could also result from a global homogeneity of the source regions. Recent works based on orbital data have shown a difference in soil S, Cl and H chemistries, especially between the northern lowlands and southern highlands, suggesting different levels of interaction with water (Hood et al., 2019), which argues against complete mixing at a global scale.

1.2 Analyses made by Curiosity at Rocknest

Increasing our knowledge of soil compositions is among the scientific objectives of the Mars Science Laboratory mission (Grotzinger et al., 2012) and its rover Curiosity. Since 2012, it has been investigating Gale crater, located south of Elysium Planitia, in the border of the Aeolis Mensae region. Its scientific payload includes tools capable of analyzing both the mineralogy and chemistry of soils. The bulk chemical composition of soils in Gale crater, measured with the Alpha Particle X-ray Spectrometer (APXS) instrument is within 2σ of the Mars Exploration Rovers (MER) analyses, except for TiO_2 (Blake et al., 2013; Morris et al., 2013; O'Connell-Cooper et al., 2017), suggesting relatively similar basaltic soils. The CheMin instrument (Blake et al., 2012), the first X-ray Diffractometer (XRD) operating on the martian surface, showed that all major mineralogical phases of the fine fraction ($<150\ \mu\text{m}$) of the Rocknest eolian soil (the Gale crater soil reference) are consistent with a basaltic source (Bish et al., 2013; Achilles et al., 2017, Morrison et al., 2018). CheMin detected igneous minerals like plagioclase ($\sim\text{An}_{50}$), olivine ($\sim\text{Fo}_{58}$) and pyroxenes (augite and pigeonite), but very few secondary products were identified and quantified. Only anhydrite ($0.9\pm 0.2\ \text{wt.}\%$), magnetite ($1.8\pm 0.3\ \text{wt.}\%$) and hematite ($1.0\pm 0.1\ \text{wt.}\%$) were observed in the X-ray diffractograms, but no clay minerals (Bish et al., 2013; Achilles et al., 2017, Morrison et al., 2018). However, CheMin analyses also revealed that $35\pm 15\ \text{wt.}\%$ of the Rocknest soil is X-ray amorphous, i.e., material that is insufficiently crystallized to be identifiable with the XRD method. The presence of amorphous phases has long been suspected on the surface of Mars (e.g., Evans and Adams, 1979; Singer, 1985; Morris et al., 2000; Milliken et al., 2008; Squyres et al., 2008), but CheMin provided the first *in situ* evidence with XRD data (Bish et al., 2013, Rampe et al., 2014). The composition of the amorphous component can be estimated with a mass balance calculation, i.e., by subtracting the chemistry of minerals identified by CheMin from the bulk chemistry measured by APXS. At Rocknest, this mass balance calculation suggests a silica-poor amorphous component ($\sim 35\ \text{wt.}\% \text{SiO}_2$), and enrichments in iron ($\sim 23\ \text{wt.}\% \text{FeO}_T$), sulfur ($\sim 14\ \text{wt.}\% \text{SO}_3$) and possibly phosphorus ($\sim 3\ \text{wt.}\% \text{P}_2\text{O}_5$) compared to the bulk crystalline composition (Blake et al., 2013; Dehouck et al., 2014; Achilles et al., 2017). The SAM (Sample Analysis at Mars) instrument (Mahaffy et al., 2012), which contains a gas chromatograph paired with a quadrupole mass spectrometer, recorded volatiles released during the heating of the Rocknest soil samples up

to ~835 °C, including H₂O, SO₂, CO₂ and O₂ (Leshin et al., 2013). The range of release temperatures suggests that water is bound to the amorphous component. The CheMin instrument did not detect any hydrated mineral in the soil, which also suggests that H₂O is associated with the amorphous component.

ChemCam, the Laser-Induced Breakdown Spectroscopy (LIBS) instrument (Wiens et al., 2012; Maurice et al., 2012), enables elementary chemistry to be determined at a sub-millimeter scale, and so is a relevant tool to constrain the chemical constituents of soils. The laser beam has a sampling area that ranges from 350 to 550 µm diameter, depending on the distance to the target. This resolution allows us to directly isolate soil components at or above some size scale, thus providing the first discrimination between different populations of grains (Meslin et al., 2013; Cousin et al., 2015). Near the landing area, some grains coarser than the laser beam were found to have predominantly a felsic composition (enriched in Si, Al, Na, and K). These grains have the same composition as rocks encountered in the Bradbury landing site and so might come from locally eroded rocks (Sautter et al., 2014; Meslin et al., 2013; Cousin et al., 2015). The second population contains grains that are both coarser and finer than the laser sampling area, with a mafic composition (enriched in Fe and Mg). The Mn, Cr and Mg signals are lower for these grains than in the neighboring rocks, suggesting a lack of direct genetic connection between these soil grains and local mafic rocks (Meslin et al., 2013; Cousin et al., 2015). ChemCam data recorded a stronger hydrogen emission peak linked to the mafic part, which may be associated with weathering products among the non-crystalline components (Meslin et al., 2013). Consequently, constraining the nature and chemistry of these hydrated amorphous phases is important to better understand the aqueous history of these sediments.

1.3 Analyses made by Curiosity in the Bagnold Dunes

The Bagnold Dunes, located near the base of Mount Sharp, are the first active dunes studied *in situ* on another planet (Bridges and Ehlmann, 2018). Two samples were scooped at different locations: Gobabeb on Sol 1225, and Ogunquit Beach on Sol 1650 (Figure 1), corresponding to the upwind and downwind margins of the dune field. The CheMin instrument was used to determine their mineralogies. They are relatively similar to that of the Rocknest sand with a crystalline part mostly composed of igneous basaltic minerals (plagioclase, olivine, augite, and pigeonite), with minor abundances of hematite, magnetite, quartz, and anhydrite (Achilles et al., 2017; Rampe et al., 2018; Morrison et al., 2018). Similarly to Rocknest, the Gobabeb and Ogunquit Beach samples have substantial fractions of amorphous materials, with respectively 35±15 (Achilles et al., 2017) and 40±15 wt.% (Rampe et al., 2018) of the bulk mineralogy. The X-ray amorphous component compositions show some differences between Gobabeb and Ogunquit Beach, especially in SiO₂ and FeO_T abundances that could be a result of different local sediment sources (Rampe et al., 2018). Second-order mixing of local bedrock contributions and mineral sorting were also observed through subtle mineralogical variation between the two locations, especially in olivine and plagioclase abundances (Achilles et al., 2017; Lapotre et al., 2017; Ehlmann et al., 2017; Rampe et al., 2018). Several scoops of the Gobabeb samples were sieved to supply portions with controlled grain sizes to the SAM and CheMin instruments. Leftovers with relatively well-constrained ranges of grain sizes were dumped onto the

ground. The Sample Acquisition/Sample Processing and Handling (Sa/SPaH) subsystem of the rover (Anderson et al., 2012) delivered four piles of the Bagnold sand: dump A (<150 μm), dump B (>150 μm), dump C (150 μm -1 mm) and dump D (>1 mm). ChemCam measurements were performed on these four different dumps (Cousin et al., 2017). Grain size distributions were also measured with ChemCam RMI images and MAHLI (Mars Hand Lens Imager) images, the latter of which has a spatial resolution better than 19 μm per pixel at a \sim 1 cm standoff distance (Edgett et al., 2013). These images reveal that no grains larger than 500 μm are detectable in piles B and C, and, as a matter of fact, no pile was formed at the expected dump D location, due to the absence of grains larger than 1 mm (Ehlmann et al., 2017). ChemCam analyses in these dump piles reveal that at least two different chemical components are present in the Bagnold Dunes. Indeed, Cousin et al. (2017) show a mixing line between two end-members: the first one is enriched in Al, Na, Si, and Ca suggesting the presence of felsic compounds, while the other one is depleted in these elements, suggesting the presence of mafic minerals, which is in agreement with CheMin mineralogy. Finally, although the hydrogen abundances recorded in the dunes were lower compared to the Rocknest soil samples (respectively 1.5-3 and \sim 1 wt.%, Leshin et al., 2013; Sutter et al., 2017; Gabriel et al., 2018), the amorphous component of the dunes is also thought to hold the H₂O content (Cousin et al., 2017; Sutter et al., 2017; Achilles et al., 2017; Ehlmann et al., 2017; Rampe et al., 2018). Similarly to Rocknest soils, constraining the origin and nature of the hydrated amorphous phases is an important step to understand the aqueous alteration processes that made the history of these soil deposits.

Figure 1: a) HiRISE mosaic of the Curiosity traverse showing the locations of the Rocknest sand and the Bagnold dunes (Gobabeb and Ogunquit Beach stops). b) MAHLI image showing the scoop locations at Rocknest (Sol 93). c) View of the Gobabeb stop in the Bagnold Dunes from one of Curiosity's front hazard avoidance cameras (Sol 1229). d) Ogunquit Beach location from the MastCam instrument. Image credits: NASA/JPL/University of Arizona (Sol 1647). (a), NASA/JPL-Caltech/MSSS (b, d), NASA/JPL-Caltech (c).

1.4 Objectives of the present study

Direct analyses of the amorphous component by ChemCam require first to understand the complexity of the interaction between the laser beam and the granular materials. The goal of this study is to conduct analyses of martian soil simulants with a replica of the ChemCam instrument in the laboratory, where experimental parameters and end-member compositions are well constrained, to better understand ChemCam flight data. Only a few studies were done on LIBS performance on non-indurated targets (see for example the review by Harmon et al., 2013), and even less under martian atmosphere conditions. Indeed, ChemCam represents the first use of the LIBS technique on another planet, and the interpretation of ChemCam data of soils is complicated in the martian environment because of the large diversity of grain sizes and the unknown physical form (i.e., the kind of grain mixtures) of soil particles, including the amorphous component. Here, we studied the interaction of the laser beam with two kinds of mixtures that occur or may occur in martian soils. The first kind corresponds to mechanical mixtures of two populations of grains of distinct chemical compositions (Figure 2, left panel). This may be applied to two populations of

crystalline grains (e.g., mafic and felsic minerals, Meslin et al., 2013; Cousin et al., 2015), but also to a population of amorphous grains mingled with crystalline grains. The second kind of mixtures that we studied corresponds to a material forming a compositionally-distinct coating at the surface of grains (Figure 2, right panel). Such a coating may be formed by the precipitation of salts from a saturated solution, for which grains can serve as nuclei. Alternatively, grains may also develop alteration rinds due to aqueous weathering processes, or get coated by dust during their transport due to electrostatic forces. Here again, the coating may be crystalline or amorphous in nature. In martian soils, these two kinds of mixtures can occur simultaneously, for example, with the mixing of primary grains, grains with secondary coatings, and fragments derived from the coatings. In addition to chemistry, constraining the physical form of the non-crystalline part is important because it can yield information about its origin and consequently result in a better understanding of the geology and aqueous history of these sediments. Dust and precipitated coatings on indurated rocks were studied previously for ChemCam data interpretation purposes (Graff et al., 2011; Lanza et al., 2015) but not with the aim of understanding soil properties. The objective of our work is to show how the LIBS technique can provide specific insight into the physical and chemical properties of soils.

Figure 2: Two types of mixtures considered in this study: mechanical mixtures of two populations of grains of distinct chemical compositions (left), or grains with a surface coating (right). The right hand panel shows that the laser beam may scatter soil grains with diameters smaller than a critical size.

In addition to hydrogen, sulfur is also an important element to study aqueous alteration processes on the martian surface. Sulfur is present in abundance in martian soils (i.e., ~6.2 wt.% SO_3 , Taylor and McLennan, 2009) mainly in the form of sulfates (e.g., King and McLennan, 2010). Sulfate minerals have been widely detected by remote-sensing (e.g., Gendrin et al., 2005; Langevin et al., 2005; Bibring et al., 2006), especially in the equatorial Valles Marineris canyon, in the adjacent Meridiani area, and in the circumpolar deposits. *In situ* analyses also reveal that sulfates correspond to abundant secondary products in martian soils. Magnesium, calcium and/or iron sulfates were identified at the Viking, Pathfinder, Phoenix and MER landing sites (e.g., Clark et al., 1993; Foley et al., 2003; Kounaves et al., 2010; Wang et al., 2006; Soderblom et al., 2004). In Gale crater soils, only anhydrite has been observed by CheMin, but the mass balance calculations indicate that sulfur is abundant in the amorphous component of the Rocknest soil with ~14 wt.% SO_3 (Achilles et al., 2017). Consequently, in this study, we also tested the sulfur LIBS emission peaks as a potential geochemical marker of S-bearing phases in martian granular media.

2. Methods

2.1. Preparation of martian analog samples

For the purpose of this study, we produced simple laboratory mixtures corresponding to the two model cases mentioned above: mechanical mixtures, and grains with a surface coating (Figure 2). Preparations were made for several grain sizes, ranging from smaller to larger than the laser beam ($\sim 425 \pm 25$ μm , Chide et al., 2019). Although this is a simplification with respect to natural martian soils, we prepared only binary mixtures to facilitate data interpretation. To enable direct comparisons between samples, the same reference was used in all kinds of mixtures: the JSC-1A lunar soil simulant (referred to as JSC-L in this paper). This glass-rich, mostly unaltered basaltic material is composed of volcanic ash from a pyroclastic sheet deposit, located in the San Francisco volcano field (McKay et al., 1994; Hill et al., 2007). It contains <1 % of olivine, feldspar and pyroxene phenocrysts. This lunar analog does not exactly match the composition of Gale crater soils (Table 1) in particular regarding the FeO_T , Al_2O_3 , CaO and SiO_2 contents but it makes an excellent basaltic volatile-poor end-member for our soil analogs because of its homogeneous composition and its low level of alteration.

Table 1: Chemical composition reference for the lunar and martian soil simulants (in wt %, volatile free and normalized). The ratio between lunar and martian simulants is calculated for all major elements. Gale soil composition from the APXS and the fine fraction of Gale soil (defined as Aeolis Palus soil) from ChemCam are also represented, as well as the Meridiani and Gusev soils (from APXS) and the average martian soil reference. Note that APXS data for Gale soils were renormalized with 2 wt.% water (similarly to Lasue et al., 2018), to enable direct comparison with ChemCam data.

| | JSC-L | JSC-M | Ratio JSC-L/JSC- M simulants | Gale soil by APXS ¹ | Gale soil by ChemCam ⁴ (Aeolis Palus) | Meridiani soil by APXS ⁵ | Gusev soil by APXS ⁵ | Average martian soil ⁶ |
|-------------------------|-------|-------|------------------------------------|-----------------------------------|---|---|---------------------------------------|---|
| SiO_2 | 46.2 | 43.5 | 1.06 | 42.61 | 42.00 | 46.1 | 46.3 | 45.41 |
| TiO_2 | 1.85 | 3.8 | 0.49 | 1.03 | 0.86 | 1.03 | 0.87 | 0.9 |
| Al_2O_3 | 17.1 | 23.3 | 0.73 | 9.19 | 8.50 | 9.38 | 10.1 | 9.71 |
| FeO_T | 11.2 | 13.88 | 0.80 | 18.36 | 18.40 | 18.10 | 15.70 | 16.73 |
| MgO | 6.87 | 3.4 | 2.02 | 8.19 | 7.70 | 7.41 | 8.60 | 8.35 |
| CaO | 9.43 | 6.2 | 1.52 | 6.88 | 7.30 | 6.94 | 6.34 | 6.37 |
| Na_2O | 3.33 | 2.4 | 1.39 | 2.75 | 1.86 | 2.23 | 3.00 | 2.73 |
| K_2O | 0.85 | 0.6 | 1.42 | 0.56 | 0.23 | 0.49 | 0.44 | 0.44 |
| MnO | 0.19 | 0.3 | 0.63 | 0.39 | - | 0.37 | 0.32 | 0.33 |
| Cr_2O_3 | - | - | - | 0.42 | - | 0.40 | 0.35 | 0.36 |
| P_2O_5 | 0.62 | 0.9 | 0.69 | 0.93 | - | 0.85 | 0.82 | 0.83 |
| SO_3 | - | - | - | 5.84 | - | 5.90 | 6.00 | 0.68 |
| Cl | - | - | - | 0.68 | - | 0.66 | 0.72 | - |
| Total | 97.64 | 100.1 | - | 97.83 | 86.85 | 99.86 | 99.56 | 99 |

¹Hill et al. (2007)

²Allen et al. (1998)

³Blake et al. (2013), updated in O'Connell-Cooper et al. (2017)

⁴Cousin et al. (2015), updated in Lasue et al. (2018)

⁵Yen et al. (2006)

⁶Taylor and McLennan (2009)

2.1.1. Mechanical mixtures

Two kinds of mechanical mixtures were prepared using the JSC-L powder, with two different volatile-bearing end-members. The first one is the JSC-1 martian regolith simulant (referred to as JSC-M in this paper). These basaltic grains are composed of altered glassy ash and cinders from the Pu'u Nene volcanic cone on Mauna Kea, Hawaii. Mineral phases present in this material include anorthite, Ti-rich magnetite, pyroxene, olivine, allophane, as well as ferrihydrite (Allen et al., 1998). Among major oxides, Al_2O_3 , FeO_T , MgO , and CaO show the most significant divergence between the martian and lunar simulants (Table 1). JSC-M is also much more altered than JSC-L and contains a higher hydrogen content. Heating for half an hour at 200°C with a thermo-balance shows that the volatile abundance (assumed to be mainly water), is greater in the bulk martian analog compared to the bulk lunar regolith simulant (respectively 11 and 1.4 wt.% materials released). The two simulants were separately sieved to produce different grain size ranges, both smaller and larger than the laser beam of the ChemCam Qualification Model used in this study ($\sim 425 \pm 25 \mu\text{m}$ at $\sim 1.8 \text{ m}$, Chide et al., 2019). The four grain size ranges used for the experiment are equivalent to $<45 \mu\text{m}$, $125\text{-}250 \mu\text{m}$, $250\text{-}500 \mu\text{m}$ and $0.5\text{-}1 \text{ mm}$. For each grain size fraction, JSC-L and JSC-M simulants were then mixed, in variable concentrations, with JSC-M abundances of 1.5, 5, 15, 25 and 50 wt.%. Only results for the fine-grained mixture ($<45 \mu\text{m}$) with 25 wt.% JSC-M are not reported here due to an autofocus issue during the LIBS analysis.

Additional mixtures were prepared using JSC-L and magnesium sulfate, to have mechanical mixtures of end-member materials also used in the coating experiments discussed later (see section 2.1.2). The use of similar materials enables us to compare the results directly between the two kinds of mixtures. Although the goal of our experiments is not to reproduce the martian soil mineralogy, magnesium sulfate was used because it was observed in other martian soils (e.g., Kounaves et al., 2010; Clark, 1993; Soderblom et al., 2004; Wang et al., 2000) and in Gale crater bedrock (e.g., Milliken et al., 2010; Fraeman et al., 2016; Rapin et al., 2019), and consequently could be a potential candidate for amorphous phases. Magnesium sulfates are also easily soluble in water, facilitating the production of coating for our experiments (see section 2.1.2). For these mechanical mixtures, we used the same concentrations as the above-mentioned JSC-M and JSC-L mixtures, but with only one range of particle sizes ($250\text{-}500 \mu\text{m}$ diameter). The thermo-balance analysis shows that the magnesium sulfate powder consisted of $\sim 31 \text{ wt.}\%$ of volatiles at ambient conditions (assumed to be mainly water). Hydration of the magnesium sulfate results from the experimental protocol used to obtain a similar material to that used in the surface coating experiments. Indeed, kieserite powder (25 g) from Sigma-Aldrich was dissolved into distilled water (100 mL). Next, the magnesium sulfate was precipitated by heating the solutions with an oven at 90°C at ambient pressure for several hours until complete evaporation of the solution. Then the resulting sulfate was crushed with an agate mortar, and

finally, sieved. While stored in a vacuum chamber at 10^{-3} mbar (see section 2.2), the end product of this protocol released the same amount of volatiles (30.6 wt.%) as the heated powder, as found by the precise weighing of the sample before and after exposure to the vacuum.

As noted above, both primary (glass) and secondary (allophane, ferrihydrite) amorphous phases are present in our end-members. These latter are probably mostly present as aggregates within other mineral phases rather than as individual grains. However, it was not our goal to try to reproduce precisely the composition of the amorphous component of the martian soil, which is not well-constrained. In addition, the crystalline or X-ray amorphous nature of the mineral constituents of the samples does not matter for our LIBS analyses, which are only sensitive to chemistry, and not to mineralogy.

2.1.2. Surface coatings

Grains with surface coatings were simulated by precipitating different amounts of magnesium sulfate (1.5, 5 and 15 wt.%) onto the JSC-L basaltic grains from a saturated aqueous solution (Figure 3.b-c). Saturation was reached by heating the solutions (distilled water with different concentrations of Mg-sulfate) containing the basaltic grains at 90°C in an oven at ambient pressure. Different grain sizes (125-250, 250-500, 500-1000 μm) of JSC-L were used as substrates for magnesium sulfate nucleation. Unlike mechanical mixtures, the finest fraction (<45 μm) was not used for this kind of samples because the decrease of inter-grain porosity did not allow efficient fluid circulation and thus decreased the coating homogeneity among grains considerably. Magnesium sulfate concentrations of 1.5 and 15 wt.% were used for the three different grain sizes (expressed here as a mass proportion between Mg-sulfate and JSC-L in the final samples). An additional concentration of 5 wt.% was also used for the 250-500 μm grain size range only. Using confocal microscopy, we roughly estimated the coating thickness to 10 ± 5 μm for 15 wt.% of Mg-sulfate deposited on basaltic grains, by focusing on the top and the bottom planes of the coating for different grain orientations.

Figure 3: Stereo-microscope images of (a) 0.5-1 mm diameter of pure grains of JSC-1 lunar soil simulant; b) 0.5-1 mm diameter of JSC-1 lunar soil simulant with a coating obtained by precipitation of 1.5 wt.% magnesium sulfate; c) 0.5-1 mm diameter of JSC-1 lunar soil simulant with a coating obtained by precipitation of 15 wt.% magnesium sulfate,

The coverage and homogeneity of the coating were estimated by pixel analysis. At least two images showing randomly chosen grains (several dozen grains per image) were acquired with a Leica S8 APO stereo-microscope for each sample. Pixels were then filtered following their red, green and blue components. Pixels belonging to uncoated basaltic surfaces were black (e.g., Figure 3.a), and the remaining pixels were attributed to the coating after removing pixels from the background. Finally, the ratio between the two populations of pixels gave the coating coverage ratio. The coating coverage for each concentration of material and grain sizes is given in Table 2.

Table 2. Coating coverage (expressed as %) of magnesium sulfate on basaltic grains of lunar soil simulant JSC-L, as a function of grain size and mixture concentration. Dash symbols correspond to mixtures that were not prepared.

| | Mg-sulfate | Mg-sulfate | Mg-sulfate |
|-----------------------|------------|------------|------------|
| | 1.5 wt. % | 5 wt. % | 15 wt. % |
| 125-250 μm | 39.2 | - | 69.2 |
| 250-500 μm | 38.2 | 55.9 | 75.1 |
| 0.5-1 mm | 37.1 | - | 79.3 |

2.2. Laboratory LIBS setup

LIBS measurements were performed with a laboratory copy of the ChemCam instrument available at the Institut de Recherche en Astrophysique et Planétologie (IRAP) in Toulouse, France. This setup allowed us to run experiments in a simulated martian environment, using the ChemCam Mast-Unit Engineering and Qualification Model (Maurice et al., 2012), and the Body-Unit Engineering Model (Wiens et al., 2012). The Nd: KGW laser emits pulsed light for 5 ns at 1067 nm to generate the plasma. The frequency of the laser used in our experiment was 1 Hz with ~ 10 mJ power on target (Maurice et al., 2012, Rapin et al., 2016). The Mast Unit instrument was operated in a climatic chamber at -20°C for best performance. The samples were analyzed at a distance of 1.8 m (similar to the distance to the calibration targets on the rover), which corresponds to a laser beam width of $425 \pm 25 \mu\text{m}$ on target (Chide et al., 2019). The telescope also collects the light emitted by the radiative decay of excited species constituting the plasma and transmits it to the three spectrometers of the Body-Unit (using 3 ms integration time), which cover the 240-906.5 nm spectral range. Samples were placed in a martian chamber (Figure 4), which allowed us to run experiments in a simulated martian atmosphere in terms of pressure (~ 7 mbar) and composition (mainly CO_2 , 1.6 % Ar and 2.7 % N_2). The gas composition and pressure have an important influence on spectral intensities, resolution and detection limits (Knight et al., 2000, Colac et al., 2004; Effenberger and Scott, 2010; Lasue et al., 2012). Before the LIBS analyses themselves, the chamber was pumped to vacuum (10^{-3} mbar) for several hours to release volatile species adsorbed on the grains. A micro-barometer inserted into the chamber enabled us to ensure that the samples were no longer degassing before introducing the simulated martian atmosphere. Then, five observations (“points”) were acquired on different locations of the sample, each corresponding to 10 laser shots for mechanical mixtures between JSC-M and JSC-L (0.5-1 mm grain sizes). All other samples were analyzed with 30 laser shots per observation point (typical of ChemCam martian measurements), which resulted in 150 spectra per sample.

Figure 4: Schematic of the ChemCam experimental setup at IRAP (EQM: Engineering and Qualification Model, EM: Engineering Model).

2.3. Data processing and ICA method

Data processing was performed the same way as for spectra collected by ChemCam on Mars (Wiens et al., 2013). For each laser burst, a passive spectrum was acquired (without laser) with the same integration

time, to remove the baseline counts of the CCD as well as ambient light reflected by the sample. Spectral noise removal and removal of the continuum linked to the Bremsstrahlung emission and free-electron recombination was done following the method presented in Wiens et al. (2013). Finally, the wavelength calibration was done by analyzing a titanium plate in similar experimental conditions. The pixel shift between spectra acquired on the titanium sample and a titanium standard (Wiens et al., 2013) was corrected on our spectra.

Similarly to the ChemCam quantification method (Clegg et al., 2017), each spectrum acquired on a geological target was normalized in different ways depending on the chemical element considered. For Fe and Mg, each pixel was divided by the standard deviation of the emission intensity whereas Si and Ca were divided by the total emission obtained on the full spectral range covered by the three spectrometers together. Conversely, for Ti, Al, Na, K, and H, each pixel belonging to the three spectral ranges was divided by the standard deviation of the emission intensity obtained on the three spectrometers separately. Instrumental effects like fluctuation in the laser irradiance due to focus quality are thereby partly corrected. However, chemical quantification from LIBS spectra is also made complex by physical and chemical matrix effects. As a result, emission peak intensities are not necessarily correlated linearly with concentrations. For example, grain sizes, cohesion, and sample roughness, as well as the thermal and optical properties of the target will directly affect the mass of ablated matter.

Major oxide quantifications on martian data use two multivariate techniques explored earlier by the ChemCam team: Partial Least Squares (Clegg et al., 2009) combined with an Independent Component Analysis (Forni et al., 2013), both using more than 400 calibration standards measured at the Los Alamos National Laboratory (Clegg et al., 2017). Such quantitative analysis cannot be fully applied in this study because of experimental constraints. Indeed, the folding mirror and the window of the climatic and martian chambers (Figure 4) induce different instrumental response functions between the flight model and the laboratory setup, and the full set of calibration standards has not been analyzed at IRAP. Consequently, as the calibration was developed for the flight model only, we are not able to easily quantify our data with this setup. Instead, we used only the Independent Component Analysis (ICA), which can be employed for qualitative analyses (and it will be shown in the next section that ICA scores behave well with concentrations in the frame of this experiment). ICA is a blind source separation method, which allows one to deconvolve pristine signals from a complex signal of several sources. Here, the sources are the contributions of each chemical element to the signal that may be considered as independent components. Ten independent components corresponding to Si, Ti, Al, Fe, Mg, Ca, Na, K, H, and Li were extracted from the martian dataset (Forni et al., 2013) by the orthogonal ICA program JADE (Joint Approximate Diagonalization of Eigenmatrices; Cardoso and Souloumiac, 1993; Cardoso, 1997). Our mixture spectra are more or less correlated with these independent components. Then, the covariance between the spectrum of a sample and each independent component gives an ICA score for each chemical element. As these covariances are linked to the chemical compositions, trends in ICA scores reflect chemical changes, which can eventually be interpreted as mineral variations when appropriate.

Sulfur is an important element to consider when studying aqueous alteration processes on Mars. However, sulfur is challenging to detect with ChemCam, because there are only a few corresponding emission lines in the spectral range covered by the three spectrometers and because of their low intensities. Moreover, the close proximity of Fe emission peaks near the sulfur ones creates interferences. In this study, we tested the sulfur emission peaks as a potential geochemical marker of S-bearing phases in martian sediments. Therefore, we extracted the three most intense sulfur peaks at 543.2, 545.5 and 548 nm from laboratory spectra of pure magnesium sulfate, and created an artificial pure sulfur spectrum that serves as an ICA component. A Pearson correlation factor can then be calculated between the empirical sulfur spectrum and the different experimental mixture spectra.

3. Results

3.1. Mechanical mixtures

3.1.1. Relationship between ICA scores and concentrations

The spectra of the three end-members used in our experiments are shown in Figure 5.a, illustrating their chemical differences. The Independent Component Analysis applied to these spectra successfully discriminated the end-member compositions. Figure 5.b represents the Fe ICA scores as a function of the Mg ICA scores obtained for the pure JSC-L, JSC-M, and magnesium sulfate samples. Although we observe some variability among the 150 shots of a given sample due to some chemical heterogeneity and intrinsic analytical repeatability, the four end-members are overall well separated. In geological terms, it means that we are able to distinguish between these different components (independently of mechanical mixtures or grain coatings), as long as we choose discriminating pairs or groups of chemical elements.

Figure 5: a) LIBS spectra obtained on the three end-members used in our experiments, to illustrate their main chemical and spectral differences. b) Mg ICA scores as a function of the Fe ICA scores for the four end-member products used in this study.

The average ICA scores obtained on JSC-L and JSC-M mixtures reveal overall linear relationships for the concentrations of all elements (Figure 6). When the concentration of JSC-M increases in the mixtures, the corresponding ICA score also increases linearly for Al, Ti, Fe and H. The same observations apply for decreases in ICA scores for Si, Mg, Na, K, and Ca, in agreement with the estimated chemical composition of the mixtures. For the larger grain sizes, some variability is observed among the mean ICA scores that can be attributed to the laser sampling of preferential minerals, unrepresentative of the bulk sample stoichiometries. Our 150 laser shots per sample enable us to approach a bulk analysis, but there is still a possible statistical bias that introduced these variabilities. Linear regressions exhibit slopes that are relatively independent of particle sizes, except for Si, Na and K. The average ICA scores for these elements show trends for the fine-

grained fraction mixtures (<45 μm) that contrasts with other particle size mixtures. The global shift toward lower values for Si (and Na and K) in this fine fraction possibly reflects chemical variations induced by the sieving process, compared to the bulk composition found in the literature (McKay et al., 1993; Allen et al., 1998, Hill et al., 2007). For example, higher olivine abundance relative to plagioclase and/or basaltic glass in the fine fraction of the JSC-L could be responsible for the decrease of the Si, Na and K ICA scores for this grain size. Similarly, the Fe-Ti oxides (ilmenite and titanomagnetite) identified in the bulk fraction (Hill et al., 2007) could be present in higher abundance in the coarser grain sizes (especially in the mixture including 1.5 wt.% JSC-M) and responsible for the increase of the Ti (and Fe) ICA score for this mixture. On the other hand, physical matrix effects due to lower grain sizes cannot be ruled out, especially for Na and K, which appear to be particularly susceptible to these effects as seen in the laboratory. Moreover, linear coefficients decrease with grain sizes for Si and K, undermining the usefulness of those two elements to discriminate mixtures for fine-grained sediments. As other elements like Al, Ti, Mg, Fe, Ca and H show ICA scores quite independent from the grain sizes used, we can conclude that these elements are less subject to physical matrix effects if present, and consequently will be used preferentially in the remainder of the article as discriminatory elements to differentiate end-member products

Figure 6: Mean ICA scores obtained for elements Si, Ti, Al, Fe, Mg, Ca, Na, K and H as a function of the JSC martian simulant in the mixtures (lower X axis) with JSC lunar simulant. The upper X axis represents the concentration (reported as oxides wt.%) estimated in the mixtures from bulk compositions (McKay et al., 1993; Allen et al., 1998, Hill et al., 2007). The average of the five observations is displayed for each sample. Red, blue, black and pink colors correspond respectively to grain sizes equivalent to: <45 μm ; 125-250 μm , 250-500 μm and 0.5-1 mm. Linear correlation coefficients between average values are also computed, expressed as R^2 , as well as the p-values. Error bars represent the standard deviation of ICA scores obtained among the 150 shots. Consequently, they reflect chemical heterogeneity within samples and intrinsic shot-to-shot repeatability of the LIBS technique, and not the error on the average.

The observation of similar linear relationships between the ICA score and concentration for all grain size ranges is particularly interesting for hydrogen because it is a marker of aqueous alteration phases. Previous works have revealed that several factors, including physical target properties, can affect the hydrogen emission peak intensities (Kurniawan et al., 2014; Schröder et al., 2015; Rapin et al., 2017a; Rapin et al., 2017b). Generally, unconsolidated targets show overall higher H peak intensities than indurated rocks. The roughness of the target as well as the gradual evolution of the LIBS crater in soil can change the laser-matter interaction (Rapin et al., 2017a; Rapin et al., 2017b). In addition to physical matrix effects between cohesive and non-cohesive materials, shot-to-shot hydrogen variability has also been observed in homogeneous indurated rocks (Rapin, 2016). The origin of this phenomenon is not yet well understood but could be linked to dehydration induced by heating from the laser pulses. But these artifacts do not seem to affect our experiments, as we did not notice any shot-to-shot trend for the hydrogen signal, and the H ICA score is found to be independent of the particle sizes of the mixtures (Figure 6.i). Consequently, the ChemCam hydrogen signal constitutes a reliable geochemical marker to distinguish materials with different hydration states in martian soils and could be used in the next section to discriminate our end-member

products. The hydrogen signal could be also particularly useful for the characterization of the amorphous component in martian soils, which is suspected to contain the H₂O content measured by the SAM and ChemCam instruments in the Rocknest soils and the Bagnold dunes since CheMin did not detect any hydrated crystalline phase in the corresponding samples (Blake et al., 2013, Bish et al., 2013, Meslin et al., 2013; Cousin et al., 2017; Achilles et al., 2017, Rampe et al., 2018, Morrison et al., 2018).

For JSC-L and magnesium sulfate mixtures, we computed the Pearson Correlation Factor (PCF) between our sulfur reference spectrum (see Methods, section 2.3) and our mixture spectra, to test the feasibility of sulfur detection by this approach. Other sulfur quantification methods are currently being developed for application to ChemCam data (e.g., Clegg et al., 2018; 2019; Rapin et al., 2019). In our experiments with magnesium sulfate, the average sulfur-PCF per sample increases linearly with increasing sulfate concentrations (Figure 7). Consequently, we show that this experimental “independent sulfur component” is successful in discriminating magnesium sulfate in our analog samples. The magnesium sulfate limit of detection (LOD), which corresponds to the lowest concentration that can be reliably detected using the sulfur peaks, with 97.5 % level of confidence (with respect to false negatives and positives), is graphically obtained following the horizontal projection from the upper prediction band (at zero magnesium sulfate content) onto the lower prediction boundary. This LOD is equivalent to ~16 wt.% MgSO₄•H₂O for a set of 150 shots (Figure 7). Interference of iron emission peaks near the sulfur ones is not responsible for the PCF trend, as the Fe content of the total mixture decreases with increasing sulfate concentration. Although JSC-L has only 10.4 wt.% iron, which is less than the iron concentration observed in Gale soils (Table 1), this result is encouraging for ongoing efforts within the ChemCam team to identify S-rich compounds in Fe-bearing matrices.

Figure 7: Pearson Correlation Factor between the sulfur spectrum and each JSC-L/magnesium sulfate mixture (250-500 μm grain sizes) as a function of the magnesium sulfate content in the mixture. The blue lines correspond to the prediction bands (at the 95% confidence level) and the green line to the 95% confidence bands obtained from the mean values. The limit of detection is graphically obtained following the horizontal projection from the upper prediction band (at zero level of magnesium sulfate content) onto the lower prediction boundary. The LOD is equivalent here to ~16 wt.% MgSO₄•H₂O. The critical level (Lc ~8 wt.% MgSO₄•H₂O) defined with respect to false positives only (at 97.5%), is obtained similarly by projecting horizontally the upper prediction boundary (at zero magnesium sulfate content), onto the linear regression. Error bars here represent the standard deviation of the ICA scores among the 150 shots (1σ). Consequently, they reflect chemical heterogeneity within samples and intrinsic shot-to-shot repeatability of the LIBS technique, and not the error on the average.

3.1.2. Effect of the grain size on the shot-to-shot variability

Hydrogen and magnesium are particularly relevant elements for discriminating JSC-L and JSC-M (Figure 8, respectively white and red dots) because the abundances of these elements are very different between both materials. For mixtures containing the same proportion of JSC-L and JSC-M but with varying grain sizes (along the vertical axis in Figure 8), we observe that the scatter of the shot-to-shot ICA scores increases with increasing grain sizes. This is also observed in Figure 6: the error bars (which correspond to

the standard deviation among the 150 shots) are larger for coarser grain sizes. This implies that the scatter of the ICA scores provides direct information on the grain size distribution. The same observations have been made for indurated rock surfaces, where the grain size distributions can be linked to the scatter in elemental compositions between observation points (Rivera-Hernandez et al., 2019). For mechanical mixtures between the two JSC simulants with grains smaller than 45 μm , we observe the lowest scatter in Mg and H ICA scores compared to other grain sizes (blue dots in Figure 8 and error bars in Figure 6.e.i), as expected. Indeed, the grain size is small enough compared to the laser beam that the measured chemical composition is equivalent to an average of the two materials, weighted by their relative concentrations. Increasing the proportion of one of the constituents shifts the entire point cloud toward the end-member of this constituent. Here we highlight that it is very difficult to extract the chemistry of all individual components mixed in a soil when their grains are smaller than 45 μm , because these components are never probed individually if well mixed. Indeed, the laser beam of our ChemCam replica is significantly larger than the grains, and consequently, all pure end-member chemistries in the sample are never reached in mixtures, as also observed by McCanta et al. (2013) on grains from indurated rocks. This is reflected in the ICA scatter plot by ICA scores of the 50 wt.% JSC-M mixture (blue dots Figure 8.c) which do not significantly overlap with the two pure materials (red and white dots Figure 8.c).

Figure 8: H ICA scores as a function of the Mg ICA scores obtained on JSC-L and JSC-M mixtures. Red and white dots represent respectively the JSC-M and JSC-L pure end-members, and blue dots correspond to mechanical mixtures. The grain size increases along the vertical axis, and the JSC-M concentration along the horizontal axis.

For grain sizes larger than 125 μm , the shot-to-shot H and Mg ICA scores start to form a mixing line between the two pure end-members for a concentration larger or equal to 5 wt.% of the JSC martian simulant (Figure 8. e, f, h, i.). In these cases, the scatter of the shot-to-shot ICA scores increases towards the minor end-member (in red). Indeed, even if the bulk compositions are overall similar among all the grain size ranges (vertical axis), the scatter of the ICA scores increases with grain size, as more data points plot along the mixing line. This is observed in Figure 6, where the mean ICA scores remain relatively constant regardless of the grain size but the shot-to-shot error-bar dispersion increases. It is an important point because it shows that even for the 125-250 μm range, i.e. smaller than the laser beam scale ($\sim 425 \pm 25 \mu\text{m}$), a mixing line emerges and reaches the two end-members. Consequently, it is possible to identify the chemistry of individual components considering the extrema of the mixing line.

A concentration of only 1.5 wt.% of JSC-M does not yield any significant influence on the scatter of the ICA scores for any of the grain sizes used. Indeed, the ICA scores for the mixtures and for the JSC-L end-member completely overlap for all the grain size ranges (blue and white dots in Figure 8. a, d, g). It can be assumed that for mixtures with grains smaller than 45 μm , the shift is too small and is masked by the dispersion of the two clusters. Therefore, the detection limit for a minor component in a binary mechanical mixture should be between 1.5 and 5 wt.%, for a soil with a chemical composition similar to the one used in our experiments. In coarse-grained mixtures (equal and over 125-250 μm), 1.5 wt.% of JSC-M is too weak to

be detectable for a set of 150 shots. In this case, it is likely a statistical limit, because grains of JSC-M are big enough to influence the LIBS signal if a shot eventually reaches one of them, but this occurs too rarely to be seen.

3.2. Coated grains

3.2.1. Fine coated-grains (<500 μm)

The second type of mixtures that we considered in this study consists of coated grains. For mixtures composed of basaltic grains smaller than 500 μm , the Fe and Mg ICA scores are highly influenced by the presence of a surface coating (Figure 9). Indeed, almost all laser shots on coated grains (blue dots in Figure 9) show a contribution from the magnesium sulfate. This can be explained by the small penetration depth of the laser per shot, combined with grain ejection at each shot due to the associated shock wave (Figure 2.b) which consequently leads to a constant replacement of ablated material. The strongest effect can clearly be seen for the highest concentration of magnesium sulfate deposited on grains, which corresponds to 15 wt.% Mg-sulfate relative to the total mass of the sample (Figure 9. b. d). Indeed, the Mg and Fe ICA scores are dominated by the composition of the superficial layer and almost completely reach the magnesium sulfate end-member. For the lowest concentration (1.5 wt.% Mg-sulfate), the influence is fainter but nevertheless present (Figure 9. a. c), as blue dots from mixtures are strongly shifted compared to white dots of the JSC-L, sulfate-free grains. The same observation was made with the 5 wt.% Mg-sulfate concentrations (see supplementary material).

The composition of the end-member coating is never totally reached in our experiment, not because the laser shots pass through the coating and probe the underlying basaltic grains, but because the coating does not cover the entire surface of the grains (Table 2), which are therefore also sampled. The coverage ratio varies strongly with the concentration of the magnesium sulfate used. Indeed, images of the samples (e.g., Figure 3. c-d) reveal that the relative areal coverage of the coated grains is only ~40 % with 1.5 wt.% Mg-sulfate and reaches ~75 % with 15 wt.% Mg-sulfate (Table 2). Consequently, in all our experiments, the basaltic substrate always influences the measurements, and this effect is dependent on the level of coating coverage (as discussed later in the section 4.2).

Figure 9: Fe ICA scores as a function of Mg ICA scores, obtained on JSC-L coated with magnesium sulfate. White and green dots represent respectively the JSC-L and magnesium sulfate pure end-members, and blue dots correspond to JSC-L coated with Mg-sulfate. The grain size increases along the vertical axis, and the magnesium sulfate concentration along the horizontal axis.

3.2.2. Coarse coated-grains (>500 μm)

The results obtained with basaltic grains larger than 500 μm coated with magnesium sulfate differ from those obtained with finer grains (see part 3.2.1). Most Fe and Mg ICA scores for mixtures with grain sizes higher than 500 μm fall close to the basaltic end-member, and only a few shots are located near the

magnesium sulfate end-member (Figure 10.a, obtained for 15 wt.% of magnesium sulfate). Moreover, by averaging the Fe ICA and Mg ICA scores by shot number, we highlight a common pattern in all LIBS observation points: a monotonic variation is observed within each burst, starting from the chemical signature of the coating in the first few shots and evolving toward the basaltic substrate end-member as the shot number increases (Figure 10.b).

Figure 10: a) Fe ICA scores as a function of Mg ICA scores obtained on JSC-L basaltic grains coated with magnesium sulfate. Grains used here range from 0.5 to 1 mm and carry 15 wt.% magnesium sulfate of the total mixture. White and green dots represent respectively the JSC-L and magnesium sulfate pure end-members, and blue dots correspond to coated JSC-L grains. b) Monotonic trends observed with depth by averaging ICA Mg scores and Fe ICA scores by shot number. Such a signature indicates the presence of coated grains. The basaltic substrate is considered as reached when ICA scores become constant (after ~10-15 shots).

This trend in ICA scores with shot number (Figure 10.b) is interpreted as a gradual removal of the coating by repeated laser ablations, with magnesium sulfate from the coating analyzed first, followed by the ablation of the basaltic grain itself. Once again, the end-member coating chemistry is never totally reached in our experiment, likely because of the imperfect coating coverage. This experiment shows that grains larger than 500 μm are coarse enough to remain in place under repeated laser shots and are not ejected by the associated shock waves, in contrast to the behavior of smaller particles. Occasional grain replacement may occur due, e.g., to the creation of a LIBS crater and grains falling into it, but averaging the results of the five observation points smoothes out these occasional events. Hence, the observed monotonic ICA score variations not only give access to the chemistry of the two compounds but can also provide a clear signature of the presence and nature of coatings at the surface of the grains. Obviously, it requires that the coating and its substrate have significant chemical differences to be observed. A similar observation was made by Lanza et al. (2012; 2015) for indurated rocks.

4. Discussion

4.1. Sulfur detection

Magnesium sulfate used in our samples is assumed to contain from 0 to ~20 wt.% H_2O , considering partial and total hydration of the pristine kieserite powder into epsomite (~51 wt.% H_2O) during the experimental precipitation process and subsequent degassing of ~31 wt.% H_2O in the vacuum of the martian chamber (see section 2.1.2). The lower limit expressed here is probably not realistic because a significant H signal is visible in the spectrum (Figure 5.a). Considering such hydration levels, our Mg-sulfate samples must contain between 53 and 67 wt.% SO_3 . Consequently, the corresponding LOD for sulfur (see section 3.1.1) is equivalent to 8.5-10.6 wt.% SO_3 . This concentration is higher than the bulk sulfur content estimated from the APXS instrument (5.48 wt.% SO_3) in the Rocknest soil (Achilles et al., 2017). It means that for a single martian soil target probed with 150 laser shots (as in our experimental conditions), sulfur is not sufficiently abundant to be detected with high confidence. However, as the LOD usually decreases as the

number of sample analyses increases, this 8.5-10.5 wt.% SO_3 threshold probably corresponds to an upper limit. From mass balance calculation, the amorphous component of martian soils contains ~14 wt.% SO_3 (Achilles et al., 2017), larger than the previously estimated sulfur LOD. This implies that our approach would allow us to confidently detect sulfur in an average ChemCam spectrum of (at least) 150 shots probing preferentially the amorphous component. This average spectrum may be built by selecting single-shot spectra showing low SiO_2 and low totals, which are the two main compositional characteristics of the amorphous component (Dehouck et al., 2018). Based on the LOD, the mass ablated by the laser needs to consist of at least 61-75 % amorphous component, which could occasionally occur based on statistics of a number of laser shots, as the amorphous component represents 35 ± 15 wt.% of the bulk soil mineralogy (Achilles et al., 2017).

4.2. Mechanical mixtures vs. coatings

Since we prepared both mechanical mixtures and coatings using magnesium sulfate, we can directly compare the sensitivity to this end-member in the two experiments. To this purpose, Figure 11 compares the Mg ICA scores obtained in both cases (i.e. mechanical mixtures and grains coatings) as a function of the actual concentration of Mg-sulfate in the samples. At the concentration of only 1.5 wt.%, the Mg score is already significantly higher for coated grains than for a mechanical mixture. It highlights the strong influence of the superficial part for grains $< 500 \mu\text{m}$ on LIBS measurements, and consequently the higher sensitivity of the LIBS technique to elements present as coatings compared to mechanical mixtures.

For grain sizes of 125-250 μm and 250-500 μm , the areal coverage of the coating increases from ~40 % with 1.5 wt.% of Mg-sulfate deposited to ~70-75 % with 15 wt.% of Mg-sulfate deposited, according to the pixel color analysis (Table 2). This means that the basaltic grain always influences the measured composition due to the heterogeneous coating of the grains in our samples. A comparison of Mg ICA scores obtained for varying surface areal coverages in coating mixtures and varying sulfate proportions in mechanical mixtures reveals a direct correlation (Figure 11). As the JSC-L and the magnesium sulfates have more or less the same density, respectively 1.55-1.95 (Hill et al., 2007) and 1.67-2.57 (considering epsomite and kieserite), areal coverage can be directly translated into a mass fraction. Indeed, for a given mass, the two products should have a relatively similar volume and thus a similar surface. In Figure 11, similar ICA scores are obtained, between a given areal coverage and the same proportion of sulfates in the mechanical mixtures. Consequently, by extrapolating, we can conclude that if the coverage was complete (and the coating thicker than the ablation depth per shot), the LIBS analysis would be fully dominated by the chemistry of the coating. This observation also confirms the good linearity of the LIBS technique and ICA analyses, i.e., the composition measured for a mechanical mixture of different components reflects the relative areal coverage of each component illuminated by the laser beam.

Figure 11: Mg ICA scores as a function of the magnesium sulfate abundance in the samples. Black diamonds represent mechanical mixtures between JSC-L and $\text{MgSO}_4 \cdot \text{H}_2\text{O}$, with grain sizes of 250-500 μm . The black dashed line corresponds to the linear

regression obtained for these points ($R^2=0.976$, $p\text{-value}=2.93E^{-5}$). The star symbols represent coated grain mixtures between JSC-L and $MgSO_4 \cdot H_2O$, with grain sizes equivalent to 125-250 μm (blue stars) and 250-500 μm (black stars). The black arrows illustrate the translation from the bulk $MgSO_4 \cdot H_2O$ concentration to the coating areal coverage, derived from image analysis. The gray dashed line corresponds to the new regression obtained considering these translated points (125-250 and 250-500 μm samples) in addition to the two pure end-members samples used in mixtures ($R^2=0.965$, $p\text{-value}=1.60E^{-4}$).

In the case of grains larger than 500 μm with full coating coverage, we can assume that considering extrema of the ICA monotonic variation (the very first shots and when ICA scores become constant, as shown in Figure 10.b) would give access to the true chemistry of the two components, i.e. the coating and the grain. The grain size threshold (500 μm) above which it is possible to observe a coating signature from a monotonic ICA score trend with shot number is likely sensitive to the experimental conditions. The main difference with martian conditions is gravity, which is almost three times smaller on Mars and thus facilitates the ejection of grains from the laser beam. Moreover, in our laboratory experiment, the laser is oriented perpendicularly to the surface of the samples (incidence angle = 0° relative to normal) because of the experiment design. On Mars, the ChemCam laser incidence angle is always higher than 0° , and the surface of the soil is seldom in the horizontal plane, which probably favors grain displacement during laser bursts. Accordingly, this 500 μm threshold should be considered as a first-order lower limit.

The correlation between coating areal coverage and mixing proportion in a mechanical mixture is important because it also demonstrates that the grain nucleus will have strictly no influence in the measurement for grains smaller than 500 μm if the coating coverage is complete and a few microns thick. Consequently, this result demonstrates that the very superficial part of the grains dominates the chemistry measured by the LIBS technique in fine soils, which can lead to an incorrect interpretation of its nature and an erroneous bulk composition of the sample. The strong influence of surface coatings on the chemistry derived by the LIBS technique is related to the small penetration depth of the laser per shot, which seems to never fully penetrate the coating in our experiments due to grain ejection. Indeed, the second important parameter is the size of the grains that are small enough to be ejected by the plasma shock wave between each shot (Figure 2b). Grain ejection leads to the continuous renewal of material between each laser shot. A gradual LIBS ablation of the coating is not possible and thus the chemistry of the grains themselves is never probed. Consequently, ChemCam chemical data, and LIBS measurements in general, can be potentially biased for fine-grained materials if coatings or alteration rinds are present.

4.3. Application to the Bagnold Dunes

Our laboratory approach is helpful to improve our understanding of the ChemCam martian dataset. Observation of grain size influences identified in this study may be used to constrain the types of mixtures that exist in martian soils.

Here we apply our laboratory results to the measurements made by ChemCam in the Bagnold Dunes, which are of particular interest because they offer the possibility to test experimental observations with a real and relatively well-constrained dataset. Indeed, this dataset is unique because it includes several targets with

varying grain size ranges. ChemCam analyses were performed on two populations of grain sizes in these dunes: grains smaller than 150 μm (dump A) and grains in the 150-500 μm size range (dump B and C). The two datasets have relatively similar statistical significance, as roughly the same number of LIBS shots were acquired (500 on dump A vs. 650 on dumps B and C). To ensure that the laser beam did not drill through the piles and hit the underlying bedrock, we checked the shot-to-shot total emission variation, which is sensitive to the nature of the targets (loose sediment vs pebble or indurated rock), as described in Meslin et al., (2013) and Cousin et al., (2015). The distance of each dump pile target from ChemCam is pretty similar ($\Delta_{\text{distances}} < 12$ cm), which ensures similar laser beam diameters. The determination of ICA scores in these dump piles reveals that at least two different chemical components are present in the Bagnold Dunes (similarly to Cousin et al., 2017). Indeed, the ICA score dispersion shows a mixing line between two end-members: the first one has a felsic composition (enriched in Al, Na, Si and Ca), while the other one is depleted in these elements, suggesting the presence of mafic minerals (Figure 12.d). As we observed two distinct grain compositions, we can first highlight that these two groups are not covered with the same coating composition (if coatings are present). As demonstrated by our laboratory experiment, the scatter of the clusters may contain information about the kind of mixture (mechanical or coating) formed by the two components. We first assume that the composition of the grains is independent of their size, as in our experiments. It is thought to be the case for the Bagnold Dunes, although the coarser fraction of the sand appears to contain a slightly higher olivine abundance (Cousin et al., 2017). We also assume that if a coating is present, the areal coverage is relatively constant across all probed grains. In the present study, we demonstrated that for coated grains smaller than 500 μm (and maybe more under martian conditions), grains are small enough to be replaced after each laser shot. Therefore, the LIBS technique gives only access to the superficial part of the soil material. Consequently, if the two chemical components of the Bagnold Dunes were present as grains with coating, the two LIBS datasets (<150 μm and 150-500 μm) should have similar ICA score dispersions, and all measured compositions should fall close to the coating end-member (as summarized in Figure 12.b). In the case of a mechanical mixture between the two components (without coating), our study shows that an increase in grain size over 125 μm leads to a transition from a small cluster of ICA scores to a mixing line between the two end-members (as illustrated in Figure 12.a).

In the Bagnold Dunes dump samples, the increase in grain sizes between the two groups (<150 μm and 150-500 μm) is also accompanied by an increase in the dispersion in the direction of the two end-members, and the average Na and Al values remain similar for the two populations of grain sizes (Figure 12.d). According to our laboratory experiments, the increase of dispersion in two directions only happens if the two components are present as a mechanical mixture. This result makes sense geologically speaking, because the two end-members observed are probably the mafic and felsic compounds detected by CheMin, and they are most likely mechanically mixed. Moreover, the RMI context image for this target (Figure 12.c) clearly shows different grain brightness from light-toned to dark-toned. Finally, these martian observations are in agreement with laboratory observations regarding the scattering of ICA scores with different grain sizes. Indeed, the scatter is smaller in Dump A compared to Dump B-C, which is consistent with smaller

grain sizes. These *in situ* observations illustrate the applicability of our experimental results to the analysis of natural samples.

Figure 12: a-b) Illustration of the ICA score scatter plot expected from two chemical elements (X and Y) discriminating two theoretical compounds in similar proportion for both mechanical mixtures (a) and coatings (b), with three ranges of varying grain sizes (<150 μm , 150-500 μm and >500 μm). The assumption is made that the X and Y elements have significantly different abundances between the two materials. In the specific case of grains greater than 500 μm with a surface coating, a compositional trend with depth is expected. That means that the recorded chemistry will go from the coating composition up to the grain composition with increasing shot number. c) ChemCam RMI image of the Bagnold Dunes dump pile A (from Sol 1229). d) Shot-to-shot Na ICA scores as a function of the Al ICA scores obtained in the Bagnold Dunes field sands for 2 sieved portions: <150 μm corresponding to dump A (red dots), and 150-500 μm corresponding to dump B and C (blue dots). Orange and magenta squares correspond respectively to average values for Dump A and Dump B-C).

4.4. Penetration depth measurement in soils

The laser penetration depth for the ChemCam instrument is estimated to be between ~ 0.3 and ~ 0.8 μm per shot from experiments made on indurated basaltic rocks (Viens, et al., 2012). Similar results were found on a basalt rock with a manganese varnish coating, with a laser penetration depth of ~ 0.3 - 0.4 μm per shot (Lanza et al., 2015). Slightly higher laser penetration depths were observed in indurated JSC-M simulants with the formation of ~ 50 μm laser pits after 5 laser shots (Chide et al., 2018). In the present study, we found a similar penetration depth of the laser in our analog soil samples as the indurated basaltic rocks. Indeed, we estimated the coating thickness to be between 5 and 15 μm (for 15 wt.% of Mg-sulfate deposited on basaltic grains). Shot-to-shot profiles on grains larger than 500 μm show that 10 to 15 shots are necessary to reach the pure substrate composition (Figure 10.b.), meaning that the sulfate coating is fully penetrated. From these observations, we can derive a penetration depth of 0.3 to 1.5 μm per shot. Consequently, we show that the laser depth penetration is similar between coarse-grained basaltic soils coated with magnesium sulfate and indurated basaltic rocks.

While LIBS measurements of the bulk chemistry of fine-grained soils may be hindered if coatings are present, the small penetration depth of the laser is, on the other hand, an advantage to detect the presence of a coating and constrain its chemistry. A comparison between the chemical compositions provided by the ChemCam and APXS instruments can also provide clues about the presence of grain coatings because of the difference in probing depths between the two techniques. For some specific elements, the APXS instrument can have a much higher penetration depth than a single shot with ChemCam (Campbell et al., 2009). Indeed, the signal measured by the APXS is a function of the attenuation level of the excitation X-rays and of those emitted by the targets. This attenuation depends on their energy and thus on the elements from which they were emitted. As an example, in a basaltic matrix, and for elements with an atomic number equal to or higher than iron ($Z \geq 26$), 90 % of the X-rays emitted by the sample come from deeper than ~ 89.3 μm (Campbell et al., 2009). The D_{90} value defined this depth above which 90 % of the detected X-rays are generated. The APXS penetration depth for such heavy elements is consequently at least sixty times larger than the

ChemCam single-pulse laser penetration depth derived above. Theoretically, in Fe-rich martian basaltic fine-grained soils with only a few microns of iron-free sulfate coating, the iron signal should be dominated by the grain contribution in the APXS measurement and thus, a high Fe content should be obtained. Conversely, the signal measured by ChemCam would be dominated by the chemistry of the coating and a low Fe content should be recorded. More generally, a significant divergence in iron concentration (or heavy elements other than iron) between both instruments would be a good indication of the presence of coatings or alteration rinds on soil grains. Such a comparison applies to a much lesser extent to low-Z elements, such as Na, Mg, Al, or Si. The penetration depth of the lightest element measured by APXS, Na, approaches that of a single laser shot of ChemCam (Campbell et al., 2009).

APXS measurements of the Rocknest sand in Gale were performed on the bulk material and a sieved fraction ($<150\ \mu\text{m}$) similar to that delivered to CheMin and SAM. Both bulk and sieved material show nearly identical chemistry except for the Ti contribution from the observation tray in the sieved fraction (Blake et al., 2013). The bulk APXS target named Portage was also analyzed by ChemCam. Previous studies have shown that the composition of the fine fraction of Rocknest soil is similar to the other fine-grained fraction of loose, unconsolidated materials found at Gale (Meslin et al., 2013; Cousin et al., 2015). Such fine-grained material is defined as Aeolis Palus soil. Figure 13 shows the chemical abundances of the Aeolis Palus soil from ChemCam measurements (blue dots), in addition to the bulk composition of the crystalline phases (red squares) and amorphous component (green diamonds) estimated from mass balance calculation using CheMin mineral phases and the bulk APXS chemistry (Achilles et al., 2017). All three datasets are normalized to the APXS bulk abundance. K and Na elements are thought to be particularly susceptible to physical matrix effects when present as a fine-grained powder, which tends to underestimate their abundances. Therefore, these elements should be used with caution. The FeO_T content measured by ChemCam of the Aeolis Palus soil is relatively similar to the bulk APXS abundance. Similarly, the TiO_2 abundance measured by ChemCam, the second heaviest element after iron ($D_{90}\sim 18.2\ \mu\text{m}$) also falls between the crystalline and the amorphous component estimations. This would imply that no coating is present around all grains, or that a coating with Fe and Ti contents similar to the grains is present. This observation suggests however that the amorphous component is not present as a coating, because it is estimated to have higher Fe and Ti contents than the crystalline component (Achilles et al., 2017), and in this case, ChemCam should “see” more iron and titanium than the bulk APXS. This would make sense from a geological perspective, as eolian processes are efficient at abrading and exfoliating the surface of grains being transported. However, we note that the uncertainties of the ChemCam measurements and of the actual Fe and Ti contents of the amorphous component derived by CheMin-APXS are large (e.g., Dehouck et al., 2014). Also, in the case of incomplete coverage of the coating, the difference between the ChemCam and APXS Fe and Ti values would be reduced. For other elements (except Na_2O), the chemical abundances recorded by ChemCam are also intermediate between the crystalline and amorphous compositions, which suggests that the amorphous component is not present at the surface of all grains but rather present as a mechanical mixture. Alternatively, it is also possible that the amorphous component may be present as a coating around some specific groups of soil grains, themselves mechanically mixed with another population of crystalline grains.

Figure 13: ChemCam chemical abundances of the Aeolis Palus soil (from Lasue et al., 2018), the fine-grained fraction of Gale soil, normalized to the bulk APXS abundances of the Portage target (from O'Connell-Cooper et al., 2017). Note that APXS data were renormalized with 2 wt.% water (similarly to Lasue et al., 2018), to enable direct comparison with ChemCam data. The accuracy of ChemCam major-element compositions is estimated by calculating the root-mean-square error of prediction (RMSE) as given by Clegg et al., 2017. The amorphous component (AmC) and crystalline bulk compositions (normalized to the bulk Portage APXS target) are also represented (* from Achilles et al., 2017). For each element, the D90 values are reported, which are the depth above which 90 % of the detected X-rays are generated (from Campbell et al., 2009).

Finally, our work provides some insight into the detectability of the amorphous component with ChemCam. The estimated proportion of the amorphous component in the Bagnold eolian soil and the Rocknest soil is 35 ± 15 wt.% (Achilles et al., 2017). Consequently, considering the uncertainties, the smallest proportion of the amorphous component expected in these soils is ~ 20 wt.%. Based on our laboratory observations, we conclude that we should be able to probe and assess the chemistry of the amorphous component by ChemCam shot-to-shot analyses if it is present as a coating (for all ranges of grain size), as well as if present as a mechanical mixture (for all ranges of grain size above 125-250 μm) with a laser beam diameter of ~ 425 μm . Our laboratory results pave the way for a full characterization of the detectability, composition and physical form of the amorphous component of Gale soils with ChemCam.

5. Conclusion

The interpretation of the ChemCam soil measurements is made challenging by the complexity of the physical interaction between the laser and the grains, but also by the diversity of grain sizes and mineral phases found in martian soils. This study aimed to produce and analyze martian soil analogs in the laboratory to better understand the effects of all these parameters. We studied two kinds of mixtures (Figure 2), each with several grain size ranges: (1) mechanical mixtures of two populations of grains of distinct chemical compositions, and (2) grains with a compositionally-distinct coating. Our experiments show that LIBS analyses of such materials are sensitive to both the type of mixture and the grain size, which in turn allows us to retrieve interesting information about the nature and composition of the sample.

First, for mechanical mixtures, we have shown that the scatter of shot-to-shot ICA scores provides information about the grain size distribution: the larger the grain size, the larger the scatter. We also showed that for mixtures of grains larger than 125 μm , elemental compositions of the two constituents can be determined by considering the extrema of the mixing line formed by the scatter of the ICA scores. Conversely, for mixtures of grains smaller than 45 μm , constraining the composition of the end-members (if well mixed) is not possible, as all measurements correspond to an average of these end-members. However, if, over a large number of analyses, the proportion of these end-members varies, they could then become detectable.

Secondly, in the case of fine coated grains (< 500 μm), our experiments show that the LIBS technique only gives access to the chemistry of the coating, due to the ejection and replacement of grains between each

shot. Consequently, soil analyses could be biased by the chemistry of a coating, if such a coating exists and covers a large fraction of the grain surfaces, and if its thickness exceeds the laser penetration depth per shot (estimated here between ~ 0.3 to $1.5 \mu\text{m}$). This can be either a difficulty or an opportunity, depending on whether one is interested in the composition of the bulk sample or in the composition of the coating.

Indeed, the small penetration depth of the laser beam can be an asset to characterize the composition of the grain coating. From our laboratory observations, the identification of a coating at the surface of grains in soils can be achieved in three different ways. First, a significant divergence in chemical abundances measured by two instruments with different sampling penetration depth (e.g., ChemCam and APXS) can suggest the presence of coated grains, although the chemical differences between the coating and underlying grains need to be significant to exceed the uncertainty of the measurements. Such a method was applied to Rocknest soil to constrain the distribution of the amorphous component in martian soil. Secondly, the lack of change in the scatter of ChemCam shot-to-shot ICA scores for different sieved fractions of the same soil sample can also enable us to detect coatings on grains. Third, in the case of coarse coated grains ($>500 \mu\text{m}$), we have demonstrated that the presence of a coating would be detectable through the observation of a monotonic trend in the shot-to-shot ICA scores, resulting from the progressive ablation of the coating first, followed by the ablation of the grain itself. Indeed, grains with sizes higher than $500 \mu\text{m}$ are coarse enough to remain immobile (no ejection) under the laser beam and thus behave as a consolidated material. Such a trend is a clear signature that would enable us to distinguish between a mechanical mixture and coated grains, although the threshold size above which grains remain immobile in the martian environment is not yet fully constrained.

The distinct signatures of mechanical mixtures and coated grains highlighted in this work could be helpful for future ChemCam studies, as well as for LIBS experiments in general. For example, we have shown that the measurements performed by ChemCam on the Bagnold Dunes dump piles were consistent with a mechanical mixture between a mafic component and a felsic component. Our results are also promising for the detection and characterization of the amorphous component of martian soils with ChemCam. Previous studies have demonstrated that the amorphous component is likely the host of the hydrogen and sulfur measured in martian soils, and we have shown here the potential of these two elements to be used as geochemical markers of alteration products in granular samples. However, regarding sulfur, future work is needed to confirm our findings, especially in a Fe-rich matrix. This could be explored with an additional sets of mixtures, more representative of martian soils. For example, MGS-1 is a good simulant for Rocknest soils with elevated iron abundance (Cannon et al., 2019). To further assess the ability to differentiate coatings and mechanical mixtures with LIBS, the use of mixing models based on predictive ICA score ratios (similar to the method followed by Usui and McSween, 2006) could also be explored. Finally future efforts should focus on the search for shot-to-shot chemical trends in the ChemCam soil dataset. Isolating the contributions of the amorphous component in these measurements would allow us to better constrain its chemical composition and physical form (i.e., coating or mechanical mixtures), and ultimately to better understand its origin.

Acknowledgments

We are grateful to the MSL science and engineering teams who operate the rover. ChemCam instrument development, operations and science support in the US were funded by the NASA Mars Exploration Program. ChemCam and MSL are supported in France by the Centre National d'Etudes Spatiales (CNES). All the ChemCam data used in this paper are released and can be found on the Planetary Data System (<https://pds-geosciences.wustl.edu/missions/msl/index.htm>). Laboratory LIBS experiments were conducted at Institut de Recherche en Astrophysique et Planétologie (IRAP) in Toulouse, France. We acknowledge the Agence Nationale de la Recherche (ANR) under the program ANR-16-CE31-0012 entitled “Mars-PRIME” for helping collaborative efforts and support for this study.

Supplementary data

Supplementary material

References

- Achilles, C. N., Downs, R. T., Ming, D., Rampe, E., Morris, R., Treiman, A., Morrison, S., Blake, D., Vaniman, D., Ewing, R., et al. (2017). Mineralogy of an active eolian sediment from the Namib dune, Gale crater, Mars. *Journal of Geophysical Research: Planets*, 122(11):2344–2361.
- Allen, C. C., Jager, K. M., Morris, R. V., Lindstrom, D. L., Lindstrom, M. M., and Lockwood, J. P. (1998). JSC Mars-1: a martian soil simulant. *Space 98*, pages 469–476.
- Anderson, R. C., Jandura, L., Okon, A., Sunshine, D., Roumeliotis, C., Beegle, L., Hurowitz, J., Kennedy, B., Limonadi, D., Mc-Closkey, S., et al. (2012). Collecting samples in Gale crater, Mars; an overview of the Mars Science Laboratory sample acquisition, sample processing and handling system. *Space science reviews*, 170(1-4):57–75.
- Bandfield, J. L. (2002). Global mineral distributions on Mars. *Journal of Geophysical Research: Planets*, 107(E6):9–1.
- Bedford, C. C., Bridges, J. C., Schwenger, J. P., Wiens, R. C., Rampe, E. B., Frydenvang, J., Gasda, P. J. (2019). Alteration trends and geochemical source region characteristics preserved in the fluvio-lacustrine sedimentary record of Gale crater, Mars. *Geochimica et Cosmochimica Acta*, 246:234–266.
- Berger, J. A., Schmidt, M. E., Gortert, R., Campbell, J. L., King, P. L., Flemming, R. L., Ming, D. W., Clark, B. C., Pradler, I., VanBommel, S. V., et al. (2016). A global Mars dust composition refined by the Alpha-Particle X-ray Spectrometer in Gale crater. *Geophysical Research Letters*, 43(1):67–75.
- Bibring, J.-P., Langevin, Y., Mustard, J. F., Poulet, F., Arvidson, R., Gendrin, A., Gondet, B., Mangold, N., Pinet, P., Forget, F., et al. (2006). Global mineralogical and aqueous Mars history derived from OMEGA/Mars Express data. *Science*, 312(5772):400–404.
- Bish, D. L., Blake, D., Vaniman, D., Chipera, S., Morris, R., Ming, D., Treiman, A., Sarrazin, P., Morrison, S., Downs, R. T., et al. (2013). X-ray diffraction results from Mars Science Laboratory: Mineralogy of Rocknest at Gale crater. *Science*, 341(6153):1238932.
- Blake, D., Vaniman, D., Achilles, C., Anderson, R., Bish, D., Bristow, T., Chen, C., Chipera, S., Crisp, J., Des Marais, D., et al. (2012). Characterization and calibration of the CheMin mineralogical instrument on Mars Science Laboratory. *Space Science Reviews*, 170(1-4):341–399.

- Blake, D. F., Morris, R. V., Kocurek, G., Morrison, S., Downs, R. T., Bish, D., Ming, D., Edgett, K., Rubin, D., Goetz, W., et al. (2013). Curiosity at Gale crater, Mars: Characterization and analysis of the Rocknest sand shadow. *Science*, 341(6153):1239505.
- Bridges, N. T., and Ehlmann, B. L. (2018). The Mars Science Laboratory (MSL) Bagnold dunes campaign, Phase I: Overview and introduction to the special issue: Bagnold dunes campaign overview. *Journal of Geophysical Research: Planets*, 123(1), 3-19.
- Brückner, J., Dreibus, G., Rieder, R., and Wänke, H. (2003). Refined data of alpha proton x-ray spectrometer analyses of soils and rocks at the Mars Pathfinder site: Implications for surface chemistry. *Journal of Geophysical Research: Planets*, 108(E12).
- Cannon, K., M., Britt, D. T., Smith, T. M., Fritsche, R. F., and Batchelor, D. (2019). Mars global simulant MGS-1: A Rocknest-based open standard for basaltic martian regolith simulants. *Icarus*, 317, 470-478, 10.1016/j.icarus.2018.08.019
- Campbell, J., Lee, M., Jones, B., Andrushenko, S., Holmes, N., Maxwell, J., and Taylor, S. (2009). A fundamental parameters approach to calibration of the Mars Exploration Rover alpha particle x-ray spectrometer. *Journal of Geophysical Research: Planets*, 114(E4).
- Campbell, J. L., Perrett, G. M., Gellert, R., Andrushenko, S. M., Boyd, M. I., Maxwell, J. A., King, P. L., and Schofield, C. D. (2012). Calibration of the Mars Science Laboratory alpha particle x-ray spectrometer. *Space Science Reviews*, 170(1-4):319–340.
- Cardoso, J.-F. and Souloumiac, A. (1993). Blind beamforming for non-gaussian signals. In *IEE proceedings F (radar and signal processing)*, volume 140, pages 362–370. IEE.
- Cardoso, J.-F. (1997). Infomax and maximum likelihood for blind source separation. *IEEE Signal processing letters*, 4(4):112–114.
- Certini, G., Karunatillake, S., Zhao, Y., Meslin, P.-Y., Cousin, A., Hood, D. R., and Scalenghe, R. (2020). Disambiguating the soils of Mars. *Planetary and space Science*, 186, 104922. 10.1016/j.pss.2020.104922
- Chide, B., Maurice, S., Murdoch, N., Lasue, J., Lousquet, B., Jacob, X., Cousin, A., Forni, O., Gasnault, O., Meslin, P.-Y., et al. (2019). Listening to laser sparks: a link between laser-induced breakdown spectroscopy, acoustic measurements and crater morphology. *Spectrochimica Acta Part B: Atomic Spectroscopy*, 153:50–60.
- Christensen, P. R., Bandfield, J. L., Smith, M. D., Hamilton, V. E., and Clark, R. N. (2000). Identification of a basaltic component on the martian surface from thermal emission spectrometer data. *Journal of Geophysical Research: Planets*, 105(E4):9609–9621.
- Clark, B. C., Baird, A., Rose, H. J., Toulmin, P., Christian, R. P., Kelliher, W. C., Castro, A. J., Rowe, C. D., Keil, K., and Huss, G. R. (1977). The Viking x-ray fluorescence experiment: Analytical methods and early results. *Journal of Geophysical Research*, 82(28):4577–4594.
- Clark, B. C. (1993). Geochemical components in martian soil. *Geochimica et Cosmochimica acta*, 57(19):4575–4581.
- Clegg, S. M., Sklute, E., Dyar, M. D., Barefield, J. E., and Wiens, R. C. (2009). Multivariate analysis of remote laser-induced breakdown spectroscopy spectra using partial least squares, principal component analysis, and related techniques. *Spectrochimica Acta Part B: Atomic Spectroscopy*, 64(1):79–88.
- Clegg, S. M., Wiens, R. C., Anderson, R., Forni, O., Frydenvang, J., Lasue, J., Cousin, A., Payre, V., Boucher, T., Dyar, M. D., et al. (2017). Recalibration of the Mars Science Laboratory ChemCam instrument with an expanded geochemical database. *Spectrochimica Acta Part B: Atomic Spectroscopy*, 129:64–85.

- Clegg, S., Anderson, R., Rapin, W., Ehlmann, B., Anderson, D., Thomas, N., Gasda, P., Frydenvang, J., Forni, O., Newsom, H., et al. (2018). ChemCam sulfur quantitative analysis and interpretation. *Lunar and Planetary Science Conference*, volume 49.
- Clegg, S., Anderson, R., Rapin, W., Ehlmann, B., Anderson, D., Thomas, N., Gasda, P., Frydenvang, J., Forni, O., Newsom, H., et al. (2019). ChemCam sulfur quantitative analysis of the Askival altered feldspathic cumulate target, gale crater, mars. *Lunar and Planetary Science Conference*, volume 50.
- Colao, F., Fantoni, R., Lazic, V., and Paolini, A. (2004). LIBS application for analyses of martian crust analogues: search for the optimal experimental parameters in air and CO₂ atmosphere. *Applied Physics A*, 79(1):143–152.
- Cousin, A., Meslin, P., Wiens, R., Rapin, W., Mangold, N., Fabre, C., Gasnault, O., Forni, O., Tokar, R., Ollila, A., et al. (2015). Compositions of coarse and fine particles in martian soils at Gale: A window into the production of soils. *Icarus*, 249:22–42.
- Cousin, A., Dehouck, E., Meslin, P.-Y., Forni, O., Williams, A. J., Stein, N., Gasnault, O., Bridges, N., Ehlmann, B., Schröder, S., et al. (2017). Geochemistry of the Bagnold dune field as observed by ChemCam and comparison with other aeolian deposits at Gale crater. *Journal of Geophysical Research: Planets*, 122(10):2144–2162.
- Dehouck, E., McLennan, S. M., Meslin, P.-Y., and Cousin, A. (2014). Constraints on abundance, composition, and nature of x-ray amorphous components of soils and rocks at Gale crater, Mars. *Journal of Geophysical Research: Planets*, 119(12):2640–2657.
- Dehouck, E., David, G., Meslin, P.-Y., Cousin, A., Gasnault, O., Forni, O., Maurice, O., and Wiens, R. C. (2018). Independent characterization of the Amorphous Component of martian soils using ChemCam LIBS data. In *Lunar and Planetary Science Conference*, volume 49.
- Edgett, K., Yingst, R., et al. (2013). Curiosity's Mars hazard lens imager (Mahli): Sol 0–179 activities, observations, range and scale characterization. *European Planetary Science Congress*, volume 8, EPSC2013–246.
- Effenberger, J. A. and Scott, R. J. (2010). Effect of atmospheric conditions on LIBS spectra. *Sensors*, 10(E5):4907–4925.
- Ehlmann, B., and Edwards, C. S. (2014). Mineralogy of the Martian surface. *Annual Review of Earth and Planetary Sciences*, 42:291–315.
- Ehlmann, B., Edgett, K., Sutter, B., Achilleos, C., Litvak, M., Lapotre, M., Sullivan, R., Fraeman, A., Arvidson, R., Blake, D., et al. (2017). Chemistry, mineralogy, and grain properties at Namib and high dunes, Bagnold dune field, Gale crater, Mars: A synthesis of Curiosity rover observations. *Journal of Geophysical Research: Planets*, 122(12):2510–2543.
- Evans, D. L. and Adams, J. B. (1979). Comparison of Viking lander multispectral images and laboratory reflectance spectra of terrestrial samples. In *Lunar and Planetary Science Conference Proceedings*, 10, 1829–1834.
- Foley, C. N., Economou, T., and Claylon, R. N. (2003). Final chemical results from the Mars Pathfinder alpha proton x-ray spectrometer: Mars exploration rover mission and landing sites. *Journal of geophysical research*, 108(E12):ROV37–1.
- Forni, O., Maurice, S., Gasnault, O., Wiens, R. C., Cousin, A., Clegg, S. M., Sirven, J.-B., and Lasue, J. (2013). Independent component analysis classification of laser-induced breakdown spectroscopy spectra. *Spectrochimica Acta Part B: Atomic Spectroscopy*, 86:31–41.
- Fraeman, A. A., Ehlmann, B. L., Arvidson, R. E., Edwards, C. C., Grotzinger, J. P., Milliken, R. E., Quinn, D. P., and Rice, M. S. (2016). The stratigraphy and evolution of lower Mount Sharp from spectral, morphological, and thermophysical orbital data sets. *Journal of Geophysical Research: Planets*, 121, 1713–1736.

- Gabriel, T., Hardgrove, C., Czarnecki, S., Rampe, E., Rapin, W., Achilles, C., et al. (2018). Water abundance of dunes in Gale crater, Mars, from active neutron experiments and implications for amorphous phases. *Geophysical Research Letters*, 45(23), 12,766-12,775. 10.1029/2018GL079045.
- Gasnault, O., Taylor, G. J., Karantillake, S., Dohm, J., Horton, N., Forni, O., Pinet, P., and Boynton, W. (2010). Quantitative geochemical mapping of martian elemental provinces. *Icarus*, 307(1):226–247.
- Gellert, R., Rieder, R., Anderson, R., Brückner, J., Clark, B., Dreibus, G., Economou, T., Klingelhöfer, G., Lugmair, G., Ming, D., et al. (2004). Chemistry of rocks and soils in Gusev crater from the alpha particle x-ray spectrometer. *Science*, 305(5685):829–832.
- Gendrin, A., Mangold, N., Bibring, J.-P., Langevin, Y., Gondet, B., Poulet, F., Bonello, G., Quantin, C., Mustard, J., Arvidson, R., et al. (2005). Sulfates in martian layered terrains: the OMEGA/Mars Express view. *Science*, 307(5715):1587–1591.
- Graff, T., Morris, R., Clegg, S., Wiens, R., and Anderson, R. (2011). Dust removal on mars using laser-induced breakdown spectroscopy. *Lunar and Planetary Science Conference*, 42.
- Grotzinger, J. P., Crisp, J., Vasavada, A. R., Anderson, R. C., Baker, C. J., Barry, F., Blake, D. F., Conrad, P., Edgett, K. S., Ferdowski, B., et al. (2012). Mars Science Laboratory mission and science investigation. *Space science reviews*, 170(1-4):5–56.
- Harmon, R. S., Russo, R. E., and Hark, R. R. (2013). Applications of laser-induced breakdown spectroscopy for geochemical and environmental analysis: A comprehensive review. *Spectrochimica Acta Part B: Atomic Spectroscopy*, 87:11–26.
- Hill, E., Mellin, M., Deane, B., Liu, Y., and Taylor, A. (2007). Apollo sample 70051 and high- and low- lunar soil simulants MLS-1A and JSC-1A: Implications for future lunar exploration. *Journal of Geophysical Research: Planets*. 112(E2). 10.1029/2006JE002767
- Hood, D., Karunatillake, S., Gasnault, O., Williams, A., Dutrow, B., Ojha, L., Kobs, S., Kim, K., Heldmann, L., and Fralick, C. (2019). Contrasting regional soil alteration across the topographic dichotomy of Mars. *Geophysical Research Letters*, 46(23): 13668-13677. 10.1029/2019GL084483
- King, P. L and McLennan, S., M. (2010). Sulfur on Mars. *Elements*, 6(2): 107-112. 10.2113/gselements.6.2.107
- Klingelhöfer, G., Morris, R. V., Berrhard, B., Schröder, C., Rodionov, D. S., De Souza, P., Yen, A., Gellert, R., Evlanov, E., Zubkov, B., et al. (2004). Jarosite and hematite at Meridiani Planum from Opportunity's Maössbauer spectrometer. *Science*, 306(5702), 1740–1745.
- Knight, A. K., Scherbarth, N. L., Cremers, D. A., and Ferris, M. J. (2000). Characterization of laser-induced breakdown spectroscopy (LIBS) for application to space exploration. *Applied Spectroscopy*, 54(3):331–340.
- Kurniawan, K. H., Tjia, M. O., and Kagawa, K. (2014). Review of laser-induced plasma, its mechanism, and application to quantitative analysis of hydrogen and deuterium. *Applied Spectroscopy Reviews*, 49(5):323–434.
- Kounave, S. P., Hecht, M. H., Kapit, J., Quinn, R. C., Catling, D. C., Clark, B. C., et al. (2010). Soluble sulfate in the martian soil at the Phoenix landing site. *Geophysical Research Letters*, 37(9). 10.1029/2010GL042613
- Langevin, Y., Poulet, F., Bibring, J. P., and Gondet, B. (2005). Sulfates in the north polar region of Mars detected by OMEGA/Mars Express. *Science*, 307(5715): 1584-1586.
- Lanza, N. L., Clegg, S. M., Wiens, R. C., McInroy, R. E., Newsom, H. E., and Deans, M. D. (2012). Examining natural rock varnish and weathering rinds with laser-induced breakdown spectroscopy for application to ChemCam on Mars. *Applied Optics*, 51(7): B74–B82.

- Lanza, N. L., Ollila, A. M., Cousin, A., Wiens, R. C., Clegg, S., Mangold, N., Bridges, N., Cooper, D., Schmidt, M., Berger, J., et al. (2015). Understanding the signature of rock coatings in laser-induced breakdown spectroscopy data. *Icarus*, 249:62–73.
- Lapotre, M. G., Ehlmann, B. L., Minson, S. E., Arvidson, R. E., Ayoub, F., Fraeman, A. A., et al. (2017). Compositional variations in sands of the Bagnold Dunes, Gale crater, Mars, from visible-shortwave infrared spectroscopy and comparison with ground truth from the Curiosity rover. *Journal of Geophysical Research: Planets*, 122(12), 2486–2509.
- Lasue, J., Wiens, R., Clegg, S., Vaniman, D., Joy, K., Humphries, S., Mezzacappa, A., Melikechi, N., McInroy, R., and Bender, S. (2012). Remote laser-induced breakdown spectroscopy (LIBS) for lunar exploration. *Journal of Geophysical Research: Planets*, 117(E1).
- Lasue, J., Cousin, A., Meslin, P.-Y., Mangold, N., Wiens, R. C., Berger, G., Dehouck, E., Forni, O., Goetz, W., Gasnault, O., et al. (2018). Martian eolian dust probed by ChemCam. *Geophysical Research Letters*, 45(20):10–968.
- Le Deit, L., Mangold, N., Forni, O., Cousin, A., Lasue, J., Schröder, S., Wiens, R. C., Summer, D., Fabre, C., Stack, K. M., et al. (2016). The potassic sedimentary rocks in Gale crater, Mars, as seen by ChemCam on board Curiosity. *Journal of Geophysical Research: Planets*, 121(5):784–804.
- Leshin, L., Mahaffy, P., Webster, C., Cabane, M., Coll, P., Conrad, P., Archer, P., Atreya, S., Brunner, A., Buch, A., et al. (2013). Volatile, isotope, and organic analysis of martian fine with the Mars Curiosity rover. *Science*, 341(6153):1238937.
- Mahaffy, P. R., Webster, C. R., Cabane, M., Conrad, P. G., Coll, P., Atreya, S. K., Arvey, R., Barciniak, M., Benna, M., Bleacher, L., et al. (2012). The sample analysis at Mars investigation and instrument suite. *Space Science Reviews*, 170(1-4):401–478.
- Mangold, N., Poulet, F., Mustard, J., Bibring, J.-P., Gondet, B., Langevin, Y., Ansan, V., Masson, P., Fassett, C., Head III, J., et al. (2007). Mineralogy of the Nili Fossae region with OMEGA/Mars Express data: 2. aqueous alteration of the crust. *Journal of Geophysical Research: Planets*, 112(E8).
- Maurice, S., Wiens, R., Saccoccio, M., Baracough, B., Gasnault, O., Forni, O., Mangold, N., Baratoux, D., Bender, S., Berger, G., et al. (2012). The ChemCam instrument suite on the Mars Science Laboratory (MSL) rover: Science objectives and mast unit description. *Space science reviews*, 170(1-4):95–166.
- McCanta, M., Dobosh, P., Dyar, M., and Newsom, H. (2013). Testing the veracity of LIBS analyses on Mars using the libssim program. *Planetary and Space Science*, 81:48–54.
- McGlynn, I. O., Fedo, C. M., and McSween, H. Y. (2012). Soil mineralogy at the Mars Exploration Rover landing sites: an assessment of the competing roles of physical sorting and chemical weathering. *Journal of Geophysical Research*, 117(E1). 10.1029/2011JE003861.
- McKay, D. S., Carter, J. L., Boles, W. W., Allen, C. C., and Allton, J. H. (1994). JSC-1: A new lunar soil simulant. *Engineering, construction, and operations in space IV*, 2:857–866.
- McSween, H. Y., McGlynn, I. O., Rogers, A., D. (2010). Determining the modal mineralogy of Martian soils. *Journal of Geophysical Research*, 115. 10.1029/2010JE003582.
- McSween, H. Y., Arvidson, R. E., Bell, J., Blaney, D., Cabrol, N. A., Christensen, P. R., Clark, B. C., Crisp, J., Crumpler, L. S., Des Marais, D., et al. (2004). Basaltic rocks analyzed by the Spirit rover in Gusev crater. *Science*, 305(5685):842–845.
- Meslin, P.-Y., Gasnault, O., Forni, O., Schröder, S., Cousin, A., Berger, G., Clegg, S., Lasue, J., Maurice, S., Sautter, V., et al. (2013). Soil diversity and hydration as observed by ChemCam at Gale crater, Mars. *Science*, 341(6153):1238670.

- Milliken, R. E., Swayze, G. A., Arvidson, R. E., Bishop, J. L., Clark, R. N., Ehlmann, B. L., Green, R. O., Grotzinger, J. P., Morris, R., Murchie, S. L., et al. (2008). Opaline silica in young deposits on Mars. *Geology*, 36(11):847–850.
- Milliken, R., Grotzinger, J., P and Thomson, B. (2010). Paleoclimate of Mars as captured by the stratigraphic record in Gale crater. *Geophysical Research Letters*. 37(4). 10.1029/2009GL041870.
- Morris, R. V., Golden, D., Bell III, J. F., Shelfer, T. D., Scheinost, A. C., Hinman, N. W., Furniss, G., Mertzman, S. A., Bishop, J. L., Ming, D. W., et al. (2000). Mineralogy, composition, and alteration of Mars Pathfinder rocks and soils: Evidence from multispectral, elemental, and magnetic data on terrestrial analogue, SNC meteorite, and Pathfinder samples. *Journal of Geophysical Research: Planets*, 105(E1):1757–1817.
- Morris, R. V., Ming, D. W., Vaniman, D., Bish, D., Chipera, S., Downs, R., Gellert, R., Treiman, A., Yen, A., et al. (2013). The amorphous component in martian basaltic soil in global perspective from MSL and MER missions. *44th Lunar and Planetary Science Conference*. #1653
- Morrison, S. M., Downs, R. T., Blake, D. F., Vaniman, D. T., Ming, D. W., Haen, R. M., et al. (2018). Crystal chemistry of martian minerals from Bradbury landing through Naukluff Plateau, Gale crater, Mars. *American Mineralogist*, 103(6), 857-871.
- Mustard, J. F., Murchie, S. L., Pelkey, S., Ehlmann, B., Milliken, R., Grant, J. A., Bibring, J.-P., Poulet, F., Bishop, J., Dobrea, E. N., et al. (2008). Hydrated silicate minerals on Mars observed by the Mars Reconnaissance Orbiter CRISM instrument. *Nature*, 454(7202):305–309.
- Nachon, M., Clegg, S., Mangold, N., Schröder, S., Kah, L., Dromart, G., Ollila, A., Johnson, J., Oehler, D., Bridges, J., et al. (2014). Calcium sulfate veins characterized by ChemCam/Curiosity at Gale crater, Mars. *Journal of Geophysical Research: Planets*, 119(9):1991–2016.
- Newsom, H. E., Crumpler, L. S., Reedy, R. C., Petersen, M. T., Newsom, G. S., et al. (2007). Geochemistry of martian soil and bedrock mantled and less mantled terrains with gamma-ray data from Mars Odyssey. *Journal of Geophysical Research: Planets*, 112(3).
- O’Connell-Cooper, C., Spray, J., Thompson, L., Gellert, R., Berger, J., Boyd, N., Desouza, E., Perrett, G., Schmidt, M., and VanBommel, S. (2017). APXS-derived chemistry of the Bagnold Dune sands: Comparisons with Gale crater soils and the global martian average. *Journal of Geophysical Research: Planets*, 122(12):2623–2643.
- Ohja, L., Lewis, K., Karunatillake, S., and Schmidt, M. (2018). The Medusae Fossae formation as the single largest source of dust on Mars. *Nature Communications*, 9, 2867. 10.1038/s41467-018-05291-5
- Pinet, P., and Chevrel, S. (1996). Spectral identification of geological units on the surface of Mars related to the presence of silicates from earth-based near-infrared telescopic CDD imaging. *Journal of Geophysical Research: Planets*, 95:14435–14446.
- Poulet, F., Bibring, J.-P., Mustard, J., Gendrin, A., Mangold, N., Langevin, Y., Arvidson, R., Gondet, B., and Gomez, C. (2005). Phyllosilicates on Mars and implications for early martian climate. *Nature*, 438(7068):623–627.
- Poulet, F., Gomez, C., Bibring, J.-P., Langevin, Y., Gondet, B., Pinet, P., Belluci, G., and Mustard, J. (2007). Martian surface mineralogy from observatoire pour la minéralogie, l’eau, les glaces et l’activité on board the Mars Express spacecraft (OMEGA/MEX): Global mineral maps. *Journal of Geophysical Research: Planets*, 112(E8).
- Rampe, E., Morris, R., Ruff, S., Horgan, B., Dehouck, E., Achilles, C., Ming, D., Bish, D., and Chipera, S. (2014). Amorphous phases on the surface of Mars. *International Conference on Mars*, volume 8.
- Rampe, E., Lapotre, M. G. A., Bristow, T. F., Arvidson, R. E., Morris, R. V., Achilles, C. N., et al. (2018). Sand mineralogy within the Bagnold Dunes, Gale crater, as observed in situ and from orbit. *Geophysical Research Letters*, 45, 10.1029/2018GL079073
- Rapin, W. (2016). Hydratation de la surface de Mars à partir des données du rover Curiosity. *PhD thesis*, Toulouse 3.

- Rapin, W., Bousquet, B., Lasue, J., Meslin, P.-Y., Lacour, J.-L., Fabre, C., Wiens, R., Frydenvang, J., Dehouck, E., Maurice, S., et al. (2017a). Roughness effects on the hydrogen signal in laser-induced breakdown spectroscopy. *Spectrochimica Acta Part B: Atomic Spectroscopy*, 137:13–22.
- Rapin, W., Meslin, P.-Y., Maurice, S., Wiens, R. C., Laporte, D., Chauviré, B., Gasnault, O., Schröder, S., Beck, P., Bender, S., et al. (2017b). Quantification of water content by laser-induced breakdown spectroscopy on Mars. *Spectrochimica Acta Part B: Atomic Spectroscopy*, 130:82–100.
- Rapin, W., Ehlmann, B., Dromart, G., Schieber, J., Thomas, N., Fischer, W., Fox, V., Stein, N., Nachon, M., Clark, B., et al. (2019). An interval of high salinity in ancient Gale crater lake on Mars. *Nature Geoscience*, 12(11):889–895.
- Rivera-Hernández, F., Sumner, D. Y., Mangold, N., Stack, K. M., Forni, O., Newsom, H., Williams, A., Nachon, M., l'Haridon, J., Gasnault, O., et al. (2019). Using ChemCam libs data to constrain grain size in rocks on Mars: Proof of concept and application to rocks at Yellowknife Bay and Pahrump Hills, Gale crater. *Icarus*, 321:82–98.
- Sautter, V., Fabre, C., Forni, O., Toplis, M., Cousin, A., Ollila, A., Meslin, P., Maurice, S., Wiens, R., Baratoux, D., et al. (2014). Igneous mineralogy at Bradbury rise: The first ChemCam campaign at Gale crater. *Journal of Geophysical Research: Planets*, 119(1):30–46.
- Schröder, S., Meslin, P.-Y., Gasnault, O., Maurice, S., Cousin, A., Wiens, R., Rapin, W., Dyar, M., Mangold, N., Forni, O., et al. (2015). Hydrogen detection with ChemCam at Gale crater. *Icarus*, 249:43–61.
- Singer, R. B. (1985). Spectroscopic observation of Mars. *Advances in Space Research*, 5(8):59–68.
- Soderblom, L. A., Anderson, R. C., Arvidson, R. E., Bell, R. E., Cabrol, N. A., Calvin, W., Christensen, P. R., Clark, B. C., Economou, T., Ehlmann, B. L., et al. (2004). Soils of Elysium crater and Meridiani Planum at the Opportunity rover landing site. *Science*, 306(5702):1723–1726.
- Squyres, S. W., Arvidson, R. E., Ruff, S., Gellert, R., Morris, R., Ming, D., Crumpler, L., Farmer, J., Des Marais, D., Yen, A., et al. (2008). Detection of silica-rich deposits on Mars. *Science*, 320(5879):1063–1067.
- Sutter, B., Mcadam, A. C., Mahaffy, P. R., Ming, D. W., Edgett, K. S., Rampe, E. B., Eigenbrode, J. L., Franz, H. B., Freissinet, C., Grotzinger, J. P., et al. (2017). Evolved gas analyses of sedimentary rocks and eolian sediment in Gale crater, Mars: Results of the Curiosity rover's Sample Analysis at Mars instrument from Yellowknife Bay to the Namib dune. *Journal of Geophysical Research: Planets*, 122(12):2574–2609.
- Taylor S. R. and McLennan, S. (2000). Planetary crusts: their composition, origin and evolution, *Cambridge Planetary Science*, 10, Cambridge University Press.
- Usui, T. and McSween, H. Y. (2007). Geochemistry of 4 Vest based on HED meteorites: Prospective study for interpretation of gamma ray and neutron spectra for the Dawn mission. *Meteoritics and Planetary Science*, 42, 255–269.
- Wang, A., Haskin, L. A., Squyres, S. W., Jolliff, B. L., Crumpler, L., Gellert, R., et al. (2006). Sulfate deposition in subsurface regolith in Gusev crater, Mars. *Journal of Geophysical Research: Planets*. 111(E2).
10.1029/2005JE002513
- Wiens, R. C., Maurice, S., Barraclough, B., Saccoccio, M., Barkley, W. C., Bell, J. F., Bender, S., Bernardin, J., Blaney, D., Blank, J., et al. (2012). The ChemCam instrument suite on the Mars Science Laboratory (MSL) rover: Body unit and combined system tests. *Space science reviews*, 170(1-4):167–227.
- Wiens, R., Maurice, S., Lasue, J., Forni, O., Anderson, R., Clegg, S., Bender, S., Blaney, D., Barraclough, B., Cousin, A., et al. (2013). Pre-flight calibration and initial data processing for the ChemCam laser-induced breakdown spectroscopy instrument on the Mars Science Laboratory rover. *Spectrochimica Acta Part B: Atomic Spectroscopy*, 82:1–27.

- Yen, A. S., Gellert, R., Schröder, C., Morris, R. V., Bell, J. F., Knudson, A. T., Clark, B. C., Ming, D. W., Crisp, J. A., Arvidson, R. E., et al. (2005). An integrated view of the chemistry and mineralogy of martian soils. *Nature*, 436(7047):49–54.
- Yen, A. S., Mittlefehldt, D. W., McLennan, S. M., Gellert, R., Bell, J. F., McSween, H. Y., Ming, D. W., McCoy, T. J., Morris, R. V., Golombek, M., et al. (2006). Nickel on Mars: Constraining on meteoritic material at the surface. *Journal of Geophysical Research: Planets*, 111(12) 10.1029/2006JE002797.

Highlights

- Mechanical mixtures and grain coatings were analyzed using LIBS in a martian atmosphere
- Grain size and concentration were varied to study their influences on LIBS signal
- We show that mixed grains or coatings have different effects on LIBS analyses
- We provide constraints on the distribution of the amorphous component in martian soil